Colloid-Brush Interactions: The Effect of Solvent Quality

A. Halperin*

Laboratoire Interdisciplinaire de Physique (UMR 5588), Université Joseph Fourier—CNRS, BP 87, 38402 Saint Martin d'Hères, France

M. Kröger*

Polymer Physics, ETH Zurich, Wolfgang-Pauli-Strasse 10, CH-8093 Zurich, Switzerland

E. B. Zhulina*

Institute of Macromolecular Compounds of the Russian Academy of Sciences, St. Petersburg, Russia

ABSTRACT: Solvent quality affects the interactions between neutral polymer brushes and colloids as manifested in the concentration profiles of the colloidal particles, $c_{prt}(z)$, and the corresponding adsorption isotherms. Lowering the solvent quality, and eventual brush collapse, reduce the osmotic pressure at height z within the brush, $\Pi(z)$, and with it the associated free energy penalty of inserting a particle into the brush, $F_{ins}(z)$. Brush collapse thus favors penetration into the brush and adsorption within it, an effect utilized in tissue engineering, chromatography etc. In the self-consistent field theory of brushes, the effect reflects both the amplitude and form of $\Pi(z)$. For good, Θ, and poor solvents, denoted by $i = g$, Θ, and p, the $\Pi(z)$ profile is $\Pi_i(z) = \Pi_i(0)u_i^{m_i}$ where H_i is the brush height and $u_i = 1 - z^2/H_i^2$. The analysis utilizes the known $m_g = 2$, $m_\Theta = 3/2$ as well as the derived $m_p = 1$ together with $\Pi_p(0)/\Pi_g(0) \sim H_p/H_g$ and $\Pi_\Theta(0)/\Pi_g(0) \sim H_\Theta/H_g$. $F_{ins}(z) \approx \Pi_i(z)R^3$ incurred by spherical particles of radius $R \ll H_i$ is significant for $R > R_{ins}(i) \sim \Pi_i^{-1/3}$ (0) where $R_{ins}(i)$ scales with the grafting density σ as $\sigma^{-4/9}$, $\sigma^{-1/2}$, and $\sigma^{-2/3}$, respectively. For non-adsorbing particles with $R \gg R_{ins}(i)$ the particles penetrate the brush to a depth of $\delta_{ins}/H_i \approx (R_{ins}(i)/R)^{r_i}$ with $r_i = 3/2, 2, 3$, and $\delta_{ins}(g) > \delta_{ins}(\Theta) > \delta_{ins}(p)$. Primary adsorption at the wall due to wall-particle contact attraction energy Ek_BT is repressed when $R > E^{1/3}R_{ins}(i)$. Ternary adsorption due to weak monomer-particle attraction is driven by a free energy scaling as $\sim\phi(z)R^2$ and thus stronger in poor solvents when the monomer volume fraction $\phi(z)$ is higher. Accordingly, the associated $c_{prt}(z)$ is high for particles large enough to accumulate k_BT or more of attractive monomer—particle contacts but small enough to avoid large $F_{ins}(z)$.
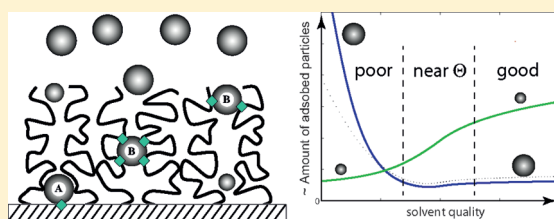
I. INTRODUCTION

The interactions between colloidal particles and polymer brushes attract interest in two domains. One involves inorganic particles and a variety of polymers and solvents having in mind composite nanomaterials and sensor applications[1-10] as well as nano-particle chromatography.[11] In the second, biotechnology domain, the particles are cells and proteins, the solvent is water and the temperatures are near ambient. Here the aim is to tune protein adsorption and cell adhesion with a view of promoting biocompatibility, harvesting cell sheets etc. In this last case special attention is given to neutral water-soluble polymers (NWSP) and in particular poly(ethylene glycol) (PEG)[12-14] and poly(N-isopropylacrylamide) (PNIPAM).[15-17] In both domains the behavior of the brush-colloid systems depend on many parameters characterizing the brushes, the particles and their interactions. These include: the area per chain, Σ, or the corresponding grafting density, $\sigma = a^2/\Sigma$ where a is the monomer size; the polymerization degree, N; the temperature, T; the shape and dimensions of the particles as well as the polymer—particle interactions. The corresponding theory and simulation efforts differed in their focus. The biotechnology

motivated studies concentrated on brushes swollen by good solvents.[6,9,10,18-28] Investigations concerned with materials applications focused on incompressible, dry melt brushes.[6,9,10] Related work addressed the atomic force microscopy force laws for swollen and melt brushes.[29-33] Little attention was given to intermediate situations occurring when the solvent quality decreases with consequent brush contraction and eventual collapse. Yet, understanding the variation of particle—brush interactions with solvent quality is of interest from two points of view. One, this is step toward a unified picture of colloid-brush interactions, from dry to highly swollen brushes. Second, understanding solvent quality effects is of practical interest in a number of situations. In the biotechnology domain, they underlie the application of thermoresponsive PNIPAM brushes in water as utilized for harvesting cell sheets[15,17,34,35] and in protein chromatography.[16] Solvent quality effects were also explored for non-aqueous solvents with the prospect of nanosensors for

the detection of organic solvents[1,2] and the development of nano-particle chromatography.[11] In addition they are of interest because block copolymer—colloid composites are typically prepared from solutions and their final state reflects intermediate states involving swollen brushes. In certain cases, even the final state is partially swollen.[36] Motivated by these observations we will consider the interactions between brushes and colloids as they vary with solvent quality focusing on the concentration of particles at altitude z within the brush, $c_{prt}(z)$. Earlier studies of brush—colloid interactions indicate that particles of larger volume tend to be expelled from the brush. However, the criterion for "large" varies with their interactions, shape, etc. As we shall discuss, it is also strongly dependent on solvent quality and a particle expelled from a brush swollen by a good solvent may penetrate a collapsed brush in a poor solvent. Our analysis utilizes the self-consistent field (SCF) theory of strongly stretched polymer brushes.[37−39] It centers on the role of the free energy penalty incurred upon inserting a particle into the brush, F_{ins}. In particular, we consider the case where F_{ins} reflects the work expended upon inserting a particle against the osmotic pressure of the unperturbed brush.[22−24] As we shall discuss, decreasing solvent quality and brush collapse lower F_{ins} thus favoring penetration into the brush and adsorption within it. Our analysis of the size effects concerns three cases often invoked in discussions of protein-brush interactions:[21] penetration of non-adsorbing particles having repulsive interactions with the wall and the polymer; particles undergoing primary adsorption solely at the wall and particles adsorbing only within the brush it self, so-called ternary adsorption (Figure 1). In all three cases, F_{ins} has the same form while the free energy driving the penetration or adsorption is different. Larger particles incur higher F_{ins} but the overall effect of size depends on the case. For example, a size range exists such that penetration is strongly repressed while primary adsorption at the wall remains significant.

Brush—colloid interactions involve numerous scenarios, and for brevity, it is necessary to limit the scope of the discussion. Two principle issues are concerned. First, in considering the theory of solvent quality effects on brush—colloid interactions it is essential to distinguish between aqueous and non-aqueous systems. A common description is possible under good solvent conditions when binary monomer—monomer interactions are dominant. However, qualitative differences can arise when the solvent quality decreases. These differences emerge when comparing neutral brushes in organic solvents and thermoresponsive NWSP brushes collapsing in water upon approaching their lower critical solution temperature (LCST). The first, "classical",[40] case is well described[41] using an interaction free energy density k_BTf_{int} with $f_{int}a^3 = \tau\phi^2 + w\phi^{3}$ [37] where $\tau = 1 - \Theta/T$ measures the deviation from the Θ temperature, $w > 0$ is a dimensionless third virial coefficient and ϕ is the monomer volume fraction. Importantly, this f_{int} does not give rise to a LCST and the description of thermoresponsive NWSP brushes requires f_{int} reflecting higher order virial terms. This distinction is important when exploring solvent quality effects because the collapse of thermoresponsive NWSP brushes can involve vertical phase separation[40,42−46] having no counterpart in classical brushes. With these observations in mind we limit our analysis to the classical case. While this discussion is strictly applicable to non-aqueous systems it also yields general insights. Furthermore, it leads to closed form analytical results and permits confrontation with computer simulations. The second issue concerns the particles mode of entry into the brush. Our discussion is limited
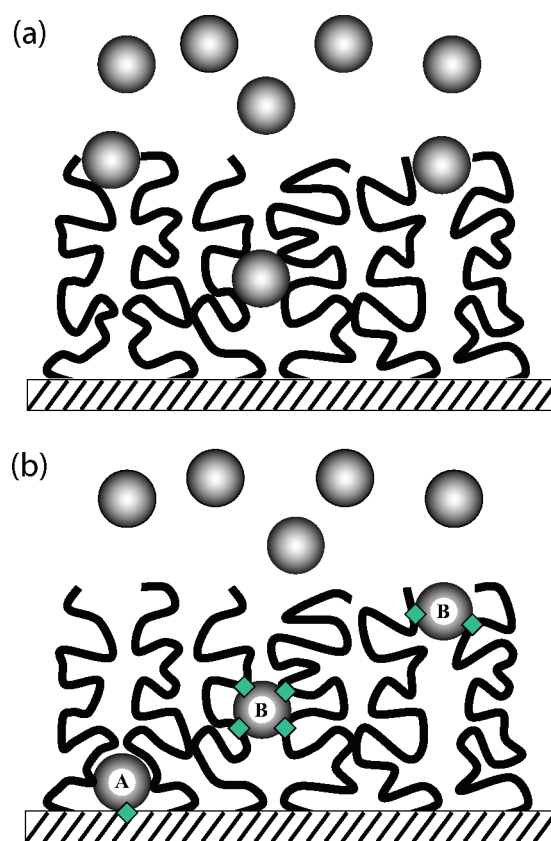
Figure 1. Contacting a dilute solution of nano particles of concentration c_b with a brush when the interaction with the polymers and the wall are repulsive. (a) Penetration into the brush is driven by translational entropy while incurring an insertion penalty thus ensuring $c_{prt}(z) < c_b$. Attractive interactions (b) with the wall or the polymer can give rise to primary (A) and ternary (B) adsorption respectively with $c_{prt}(z) > c_b$. Attractive contact interactions are schematically depicted by green diamonds.

to particles whose insertion into the brush induces only local perturbation of the monomer concentration profile.[25,27,30] This scenario, supported by computer simulations, is realized in swollen brushes when two requirements are fulfilled: (a) The particle—monomer interactions are either repulsive or weakly attractive, thus ruling out the formation of dense monomer layer around the particle.[47] Note that repulsive interactions do not rule out penetration into the brush or adsorption at the wall. (b) The particle is small enough to allow chain trajectories to circumvent it. When these conditions are satisfied, F_{ins} is related to the osmotic pressure within the brush

$$F_{ins}(z) = \int_0^H \Pi(z')A(z,z')\,dz' \qquad (1)$$

where $A(z,z')\,dz'$ is the cross sectional volume at z' of the particle whose geometrical center is at altitude z, $\Pi(z)/k_BT = \phi\,\partial f_{int}/\partial\phi - f_{int}$ is the osmotic pressure of a bulk solution with a monomer volume fraction $\phi = \phi(z)$ and H is the brush height where $\Pi(H) = 0$. The definition of "small enough" depends on the particle's geometry. For spherical particles of radius R it implies $R \ll H$. Our analytical, approximate results concern this case, when $\Pi(z)$ varies slowly over a z interval comparable to R and a particle at z incurs $F_{ins}(z) \approx \Pi(z)V$ scaling with the particle volume $V \approx R^3$.

However, the plots depicted in the figures are obtained using eq 1 and include numerical factors omitted in the body of the text. Finally, note that the formulation of the theory problem depends somewhat on the system considered. Biotechnology applications often involve contact with multicomponent biological fluids containing proteins of different size, shape and interactions. In such situations the focus is on optimizing Σ and N.[18−24] In contrast, the formulation of nano composites allows to tune R of inorganic colloids while keeping their interactions constant. As a result theories motivated by such systems consider the effect of varying R.[6,9,10] Since our discussion concerns classical brushes and non-aqueous solvents we follow the second route.

An analytical closed form formulation allowing to study solvent quality effects on F_{ins} requires knowledge of $\Pi(z)$ in Θ as well as in asymptotically good and poor solvents, denoted in the following by $\Pi_\Theta(z)$, $\Pi_g(z)$, and $\Pi_p(z)$, respectively. While $\Pi_g(z)$ and $\Pi_\Theta(z)$ are established, to our knowledge $\Pi_p(z)$ was not obtained thus far. Accordingly we first derive $\Pi_p(z)$ in poor solvent utilizing the SCF theory of polymer brushes. With this $\Pi_p(z)$ at hand, the SCF $\Pi(z)$ profiles in good, Θ and poor solvents manifest two leading features: (i) $\Pi_\Theta(0)/\Pi_g(0) \sim H_\Theta/H_g < 1$ and $\Pi_p(0)/\Pi_g(0) \sim H_p/H_g \ll 1$ thus indicating that $F_{ins}(z)$ increases with H and the solvent quality and is lowest for a collapsed brush. (ii) The $\Pi(z)$ profiles sharpen as the solvent quality diminishes and their range decreases. The solvent dependent $F_{ins}(z)$ fully determines $c_{prt}(z)$ of non-adsorbing particles penetrating the brush because of translational entropy gain, where $c_{prt}(z) \sim \exp[-F_{ins}(z)/k_BT]$. When the particles adsorb, $c_{prt}(z)$ reflects the interplay between $F_{ins}(z)$ and the attractive free energy driving the adsorption, $F_{att}(z)$. The detailed features of the resulting $c_{prt}(z)$ vary with the nature of $F_{att}(z)$, be it contact particle-wall attraction, monomer-particle attraction or another interaction. In all cases we consider monodispersed planar brushes with uniform Σ at equilibrium with a dilute solution of monodispersed spherical particles of radius R. Our discussion concerns "pure" scenarios: penetration, primary adsorption and ternary adsorption. This approach allows to clearly identify the characteristic R's controlling $c_{prt}(z)$ in each case. The real situation may well involve a combination of the three considered scenarios as well as additional contributions. However, in the dilute limit the different contributions are roughly additive and our results can be generalized accordingly.

The remainder of the article is organized as follows. The analytical SCF theory results concerning $\phi(z)$ and $\Pi(z)$ of classical brushes in good, Θ and poor solvents are summarized in section II. Section III addresses the penetration of non-adsorbing particles into swollen brushes and its variation with solvent quality. Solvent quality effects on primary adsorption[48] at the wall[19,21−23] are briefly discussed in section IV while the effects on ternary adsorption[21] due to weak monomer-particle attraction[20,21,23,24] are considered in section IV. The Discussion presents an overview of our results and their limitations as well as a summary of relevant simulations and experiments. Technical details of the SCF theory are delegated to an Appendix A. It also contains an interpolation formula for the brush swelling ratio utilized in the numerical calculations. The SCF penetration depth of non-adsorbing particles is considered in Appendix B. Certain details of the ternary adsorption case are discussed in Appendices C−E. Appendix F describes
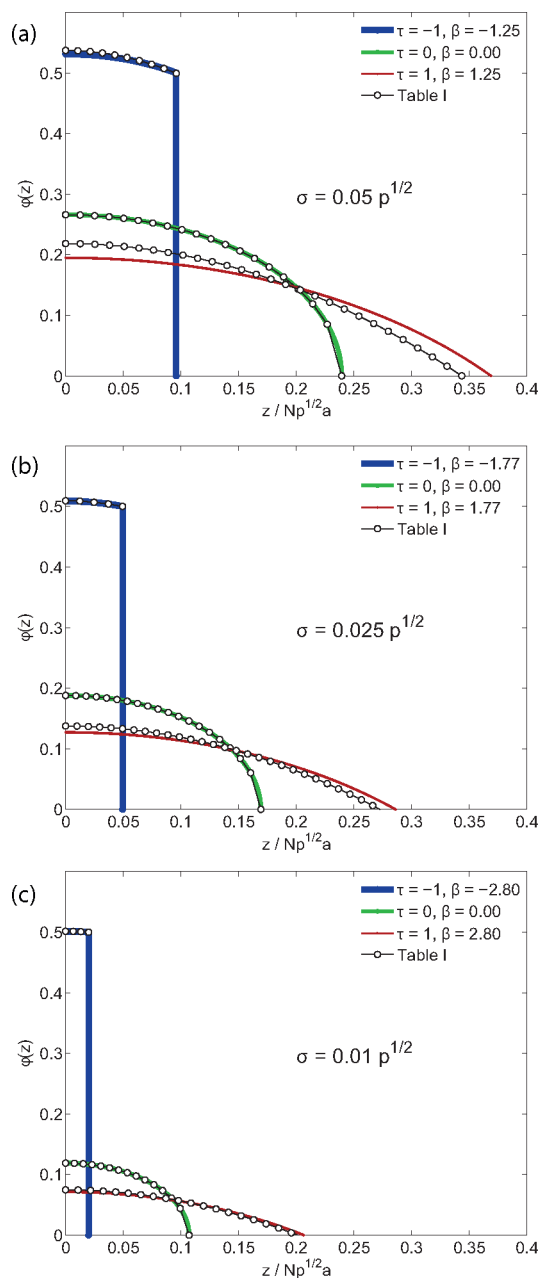
Figure 2. $\phi(z)$ vs reduced height $z/Np^{1/2}a$ for a classical brush at good, Θ and poor solvent conditions as obtained at $\tau = 1$, 0, and -1 with $w = 1$ and for $\sigma/p^{1/2} = 1/20$ (top) $\sigma/p^{1/2} = 1/40$ (middle), and $\sigma/p^{1/2} = 1/100$ (bottom). The β values are obtained via eq 3. Exact numerical solutions of the SCF equations (Appendix F) depicted by colored lines are compared to the asymptotic $\phi(z)$ in Table 1 (black -o-o-o-).

the numerical route for producing the results shown in the plots.

II. ON $\phi(z)$ AND $\Pi(z)$ WITHIN THE SCF THEORY

In this section, we will summarize with some extensions the analytical SCF results concerning $\phi(z)$ and $\Pi(z)$ for semidilute classical brushes. These results will be invoked later in our discussion of solvent quality effects on the interactions between brushes and colloidal particles. Our presentation follows the

Table 1. Asymptotic Regimes and Θ Behavior of the Monomer Volume Fraction $\phi(z)$ of a Classical Brush[a]

solvent quality(i)		$\phi(z)$	$\phi(z = 0)$	H_i
good	$\beta \gg 1$	$\phi_g u(z/H_g)$	$\phi_g = (3\pi^{2/3}/4)(p\tau)^{-1/3}\sigma^{2/3}$	$H_g = (8/\pi^2)^{1/3}Na(p\tau\sigma)^{1/3}$
Θ	$\beta = 0$	$\phi_\Theta u^{1/2}(z/H_\Theta)$	$\phi_\Theta = (2/wp)^{1/4}\sigma^{1/2}$	$H_\Theta = (4/\pi)Na(wp/2)^{1/4}\sigma^{1/2}$
poor	$\beta \ll -1$	$\bar{\phi}_p[1 + (\pi^2/54\beta^4)u(z/H_p)]$	$\phi_p = \bar{\phi}_p(1 + \pi^2/54\beta^4) \approx \bar{\phi}_p$	$H_p = Na(\sigma/\bar{\phi}_p)(1 - \pi^2/81\beta^4)$

[a] ϕ_i and H_i denote the values of $\phi(z = 0)$ and H for Θ solvents as well as for asymptotically good ($i = g$) and poor ($i = p$) ones. The behavior for $0 < |\beta| \ll 1$ is discussed in Appendix A containing an approximation of $H(\beta)$ for all β as given by eq A21.

Table 2. Asymptotic good and poor solvent regimes and the Θ behavior of $\Pi(z)$ of a classical brush

solvent quality		$\Pi_i(z)$	$\Pi_i(0)a^3/k_BT$
good	$\beta \gg 1$	$\Pi_g(0)u^2(z/H_g)$	$(9\pi^{4/3}/16)\tau^{1/3}p^{-2/3}\sigma^{4/3}$
Θ	$\beta = 0$	$\Pi_\Theta(0)u^{3/2}(z/H_\Theta)$	$2^{7/4}w^{1/4}p^{-3/4}\sigma^{3/2}$
poor	$\beta \ll -1$	$\Pi_p(0)u(z/H_p)$	$(3\pi^2/8\bar{\phi}_p)p^{-1}\sigma^2$

approach of[37] with modifications in the case of the poor solvent asymptote. The detailed derivation, with an extended discussion of the near Θ regime, is given in the Appendix A. Irrespective of solvent quality, the monomer concentration profile $\phi(z)/a^3$ within the brush is specified in terms of

$$u \equiv u(z/H) = 1 - z^2/H^2 \qquad (2)$$

where $H = H(\beta)$ is the equilibrium height as determined by

$$\beta \equiv \frac{\tau p^{1/4}}{3 \times 2^{1/4} \times w^{3/4}\sigma^{1/2}} \qquad (3)$$

and p is the number of monomers in a persistent segment. Notice that β depends on the solvent quality as characterized by $\tau \equiv 1 - \Theta/T$ and w as well as on the brush grafting density σ. $\beta = 0$ corresponds to a Θ solvent while asymptotically good and poor solvent behavior are obtained at $\beta \gg 1$ and $\beta \ll -1$ respectively. Note further that varying σ is subject to to the constraint that strong chain crowding is maintained in the τ range of interest. The asymptotic regimes, corresponding to $|\beta| \gg 1$, and the Θ behavior (Figure 2) are summarized in Table 1.

The poor solvent expressions elaborate earlier results[37] that approximated the collapsed $\phi(z)$ as a step-like with $\phi(z) \simeq \bar{\phi}_p = |\tau|/2w$ corresponding to the monomer volume fraction in a collapsed globule. While the leading behavior of $\phi(z)$ is of the form $\phi(z) = \phi_i(z = 0)u^{n_i}(z/H_i)$ with $n_g = 1$, $n_\Theta = 1/2$, and $n_p = 0$ the modified poor solvent $\phi(z)$ incorporates a higher order correction essential for the correct calculation of $\Pi(z)$. The osmotic pressure profiles for $\Pi(z)$, as obtained from local force balance within the brush (see Appendix A, eqs A10 and A11) are of the form $\Pi_i(z) = \Pi_i(0)u^{m_i}(z/H_i)$ with $m_g = 2$, $m_\Theta = 3/2$, and $m_p = 1$, as specified in Table 2 (Figure 3).

These expressions are identical to the ones obtained from $\Pi/k_BT = \phi\partial f_{int}/\partial\phi - f_{int}$: for a good solvent $\Pi_g(z)a^3/k_BT = \tau\phi^2(z)$, for Θ solvent $\Pi_\Theta(z)a^3/k_BT = 2w\phi^3(z)$ and for a poor solvent $\Pi_p(z)a^3/k_BT = -|\tau|\phi^2(z) + 2w\phi^3(z)$. This last expression for $\Pi_p(z)$ highlights the role of the $(1 + \pi^2u/54\beta^4)$ factor in $\phi(z)$: constant, u independent, terms cancel out leading to $\Pi_p(z) \sim u(z/H_p)$. The approximation of $\phi(z)$ by $\phi(z) \approx \bar{\phi}_p$ leads, in contrast, to $\Pi_p(z) = 0$. Note that $\Pi(\phi = \bar{\phi}_p) = 0$ corresponds to a collapsed globule of infinite size coexisting with pure solvent,[49] a situation involving no chain stretching. In the brush, this condition occurs only at $z = H_p$ since in the correct form $\phi_p(z < H_p) > \bar{\phi}_p$.
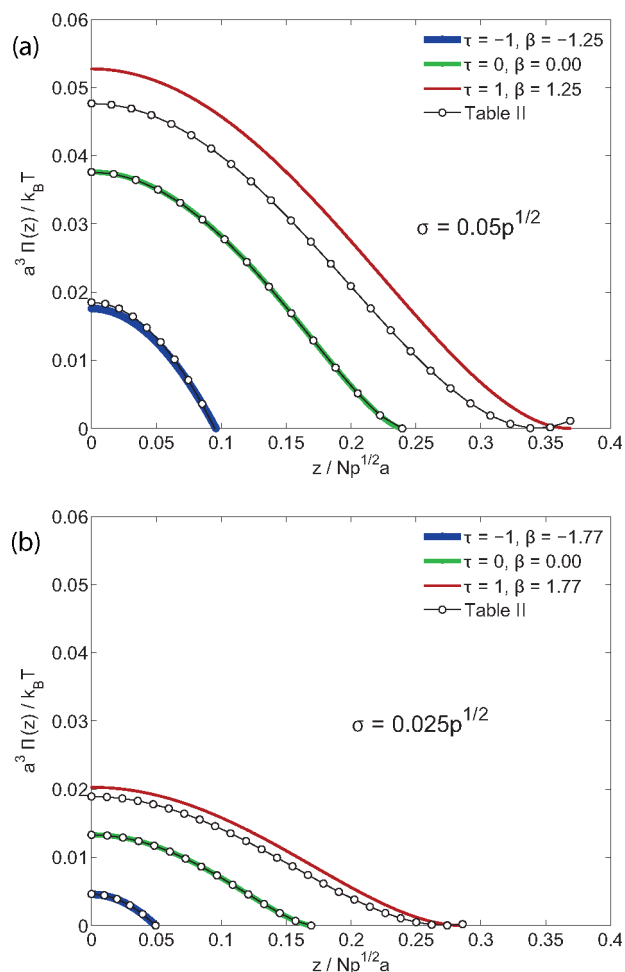
Figure 3. $\Pi(z)a^3/k_BT$ vs $z/Np^{1/2}a$ profiles for a classical brush at good, Θ and poor solvent conditions as obtained at $\tau = 1, 0,$ and -1 with $w = 1$ for $\sigma/p^{1/2} = 1/20$ (top) and $\sigma/p^{1/2} = 1/40$ (bottom). Exact numerical solutions of the SCF equation (Appendix F) depicted by colored lines are compared to the asymptotic forms given in Table 2 (black -o-o-o) Note that while the $\phi(z)$ at $\tau = -1$ are essentially step like the corresponding $\Pi(z)$ are parabolic.

In every case, the SCF $\Pi_i(z)$ is monotonically decreasing and the scale of $F_{ins} \approx \Pi_i(z)R^3$ is set by $\Pi_i(0)$. In turn, the effect of solvent quality on F_{ins} is visible from the H-dependence of $\Pi(0)$

$$\frac{\Pi_p(0)}{\Pi_g(0)} = \frac{4}{3}\frac{H_p}{H_g}, \quad \frac{\Pi_\Theta(0)}{\Pi_g(0)} = \frac{32}{9\pi}\frac{H_\Theta}{H_g} \qquad (4)$$

Since $H_g > H_\Theta > H_p$, eq 4 leads to $\Pi_p(0) < \Pi_\Theta(0) < \Pi_g(0)$. Finally, it is useful to note that the Θ behavior is relevant not only

for $\beta = 0$ but also for the $0 < |\beta| \ll 1$ range. In this regime the interior of the brush exhibits Θ solvent $\phi(z)$ and $\Pi(z)$ profiles while the exterior manifests either good or poor solvent behavior, depending on τ. Accordingly, one may estimate F_{ins} by $F_{ins}(z) \approx \Pi_{\Theta}(z)R^3$ when $0 < |\beta| \ll 1$ and $z \ll H$.

III. BRUSH PENETRATION BY NON-ADSORBING PARTICLES

Nonadsorbing particles penetrate into the brush because of the associated gain in translational entropy. In this situation, the particle concentration profile, $c_{prt}(z)$, is determined by $F_{ins}(z)$ alone. The discussion of this case provides a basis for the analysis of adsorption scenarios where $F_{ins}(z)$ competes with an additional attractive free energy as described in subsequent sections. It is also of interest being the least time-consuming case to simulate and because of its relevance to the description of the interactions between proteins and NWSP brushes. This situation was theoretically analyzed by Kim and O'Shaughnessy for dry brushes.[6] For brushes swollen by good solvent the phenomenon was studied by Yaneva et al.[28] using molecular dynamics simulations. Here we consider the penetration of non-adsorbing particles into swollen brushes as it varies with solvent quality. We focus on the case of spherical particles of radius $R \ll H_i$ such that their insertion into the brush perturbs the monomer concentration only locally. In this limit, $\Pi(z)$ experienced by the particle is roughly constant and $F_{ins}(z) \approx \Pi_i(z)V \approx \Pi_i(z)R^3$. For simplicity we limit the discussion to dilute bulk solutions with concentration c_b such that the corresponding chemical potential is $\mu_{bulk} = k_B T \ln c_b$.[50] The chemical potential of an inserted particle is $\mu(z) = k_B T \ln c_{prt}(z) + F_{ins}(z)$, and the equilibrium condition $\mu_{bulk} = \mu(z)$ thus leads to

$$c_{prt}(z) \approx c_b \exp\left[-\frac{\Pi_i(z)R^3}{k_B T}\right] < c_b \qquad (5)$$

i.e., $c_{prt}(z)$ varies as $\Pi(z)$ changes with the solvent quality . In the SCF regimes considered $\Pi_i(z) = \Pi_i(0)u^{m_i}(z/H_i)$ with $m_g = 2$, $m_{\Theta} = 3/2$ and $m_p = 1$ (Table 2), and $\Pi_i(z)$ is a monotonically decreasing function attaining its maximum at the wall. $F_{ins}(z) \approx \Pi_i(z)V$ is well-defined in the range $R \leq z < H$ since the center of the hard core particle is excluded from $0 \leq z < R$. It is however useful to introduce $F_{ins}(0) \approx \Pi_i(0)V$ because this sets the scale of $F_{ins}(z)$. In particular, $F_{ins}(z)$ affects $c_{prt}(z)$ only when $F_{ins}(0) > F_{ins}(z) > k_B T$. It is thus useful to define a solvent quality dependent characteristic R, R_{ins}, via the condition $F_{ins}(0) = k_B T$. For Θ solvents and the asymptotic $|\beta| \gg 1$ regimes, this leads to

$$R_{ins}(i) \approx \left[\frac{k_B T}{\Pi_i(0)}\right]^{1/3} \qquad (6)$$

When $R > R_{ins}(i)$, the particle experiences $F_{ins}(z) > k_B T$ at certain z values while $F_{ins}(z) < k_B T$ at all altitudes for $R < R_{ins}(i)$. F_{ins} can be expressed compactly in terms of $R_{ins}(i)$ in the form $F_{ins}(z) \approx (R/R_{ins}(i))^3 u^{m_i}(z/H_i)$ thus leading to

$$c_{prt}(z) \approx c_b \exp\left[-\left(\frac{R}{R_{ins}(i)}\right)^3 u^{m_i}(z/H_i)\right] \qquad (7)$$

with

$$R_{ins}(i) \sim \begin{cases} \tau^{-1/9}\sigma^{-4/9} & \text{good solvent :} \quad \beta \gg 1 \\ \sigma^{-1/2} & \Theta \text{ solvent :} \quad \beta = 0 \\ |\tau|^{1/3}\sigma^{-2/3} & \text{poor solvent :} \quad \beta \ll -1 \end{cases} \qquad (8)$$

Accordingly, $R_{ins}(p) > R_{ins}(\Theta) > R_{ins}(g)$, indicating that penetration is facilitated when the solvent is poorer (Figure 4). For a poor solvent, when $m_p = 1$, these equations are essentially identical to the dry brush result as given in eqs 17 and 18 of Kim and O'Shaughnessy.[6] The behavior in good and Θ solvents is different but in every case the effect on $\exp(-F_{ins}/k_B T)$ is characterized by the ratio $(R/R_{ins}(i))^3$. Importantly, the particles are depleted from regions with $F_{ins}(z) > k_B T$. The span of the depletion region, $z_{dep}(i)$ depends on solvent quality and is roughly defined by $F_{ins}[z_{dep}(i)] \approx k_B T$ leading to

$$z_{dep}(i) \approx \begin{cases} H_g\sqrt{1 - \left(\frac{R_{ins}(g)}{R}\right)^{3/2}} & \text{good solvent} \\ H_{\Theta}\sqrt{1 - \left(\frac{R_{ins}(\Theta)}{R}\right)^2} & \Theta \text{ solvent} \\ H_p\sqrt{1 - \left(\frac{R_{ins}(p)}{R}\right)^3} & \text{poor solvent} \end{cases} \qquad (9)$$

There is no depletion region for $R \leq R_{ins}(i)$ and its span approaches H_i as R increases beyond $R_{ins}(i)$. The $c_{prt}(z)$ profiles are rather insensitive to τ when $R < R_{ins}(i)$. The effect of τ increases for $R > R_{ins}(i)$ being strongest for good solvent where $c_{prt}(z)$ is depleted beyond H_g because of the penalty associated with partial insertion. The effect of solvent quality is clearest for a given intermediate R. Thus, particles with $R_{ins}(\Theta) < R < R_{ins}(p)$ penetrate a collapsed brush while being largely expelled from a brush swollen by a good solvent (Figure 4).

The characteristics of the depletion region assume simpler forms in the $R \gg R_{ins}(i)$ limit. In this case the particles are excluded from most of the brush and their penetration is limited to an exterior region of depth $\delta_{ins}(i) = H_i - z_{dep}(i)$. The expressions for δ_{ins} and the corresponding $c_{prt}(z)$ are cited below in order facilitate comparison with the results of Kim and O'Shaughnessy for dry brushes[6] and highlight the effects of solvent quality within the SCF theory. These results are also of possible interest because of simulations studies concerning particle depletion.[28,51] It is however useful to first note the difficulties inherent to the SCF analysis of this regime. The first problem is that the description of shallow penetration within the SCF theory is delicate because the strong stretching assumption is not applicable at the outer edge of a finite brush where fluctuations become important. In particular, $\phi(z)$ at the outer edge deviated from the SCF predictions and exhibits weak tail of longer range. Similar deviations are expected for the SCF $\Pi(z)$ profiles. In addition, recent simulations[25] support $F_{ins}(z) \approx \Pi(z)R^3$ for deeply inserted particles but indicate that additional contributions play a role at the outer edge of the brush. These two observations suggest caution in utilizing SCF theory and eq 1 or $F_{ins}(z) \approx \Pi(z)R^3$ to discuss the $H_i \gg R \gg R_{ins}(i)$ limit. With this caveat we note that eq 9 yields in this limit a penetration

depth $\delta_{\text{ins}}(i) = H_i - z_{\text{dep}}(i)$

$$\delta_{\text{ins}}(i) \approx \begin{cases} \dfrac{H_g}{2}\left(\dfrac{R_{\text{ins}}(g)}{R}\right)^{3/2} & \text{good solvent} \\[2ex] \dfrac{H_\Theta}{2}\left(\dfrac{R_{\text{ins}}(\Theta)}{R}\right)^{2} & \Theta \text{ solvent} \\[2ex] \dfrac{H_p}{2}\left(\dfrac{R_{\text{ins}}(p)}{R}\right)^{3} & \text{poor solvent} \end{cases} \quad (10)$$

Combining eq 4 with $R_{\text{ins}}(i) \approx [k_B T/\Pi_i(0)]^{1/3}$ leads, in this limit, to $\delta_{\text{ins}}(p)/\delta_{\text{ins}}(g) \approx [3H_p R_{\text{ins}}^3(p)/4H_g R^3]^{1/2} < 1$ and to $\delta_{\text{ins}}(\Theta)/\delta_{\text{ins}}(g) \approx [9\pi H_\Theta R_{\text{ins}}(\Theta)/32H_g R]^{1/2} < 1$ and thus to $\delta_{\text{ins}}(g) > \delta_{\text{ins}}(\Theta) > \delta_{\text{ins}}(p)$. The penetration length thus increases with increasing solvent quality, as opposed to the trend noted with respect to penetration of the interior of the brush as manifested in $R_{\text{ins}}(p) > R_{\text{ins}}(\Theta) > R_{\text{ins}}(g)$. The variation in $\delta_{\text{ins}}(i)$ reflects a "tail" effect. In particular, the slope of the peripheral part of $\Pi(z)$ decreases as the solvent quality increases. The corresponding concentration profiles at the vicinity of the edge, $z \lesssim H_i$, are

$$\frac{c_{\text{prt}}(z)}{c_b} \approx \begin{cases} \exp\left[-\left(\dfrac{H_g - z}{\delta_{\text{ins}}(g)}\right)^{2}\right] & \text{good solvent} \\[2ex] \exp\left[-\left(\dfrac{H_\Theta - z}{\delta_{\text{ins}}(\Theta)}\right)^{3/2}\right] & \Theta \text{ solvent} \\[2ex] \exp\left[-\left(\dfrac{H_p - z}{\delta_{\text{ins}}(p)}\right)\right] & \text{poor solvent} \end{cases} \quad (11)$$

Finally, when $\delta_{\text{ins}}(i) \approx R$ the particles are essentially excluded to the brush's outer boundary thus defining a maximal, solvent dependent $R_{\text{max}}(i)$ permitting penetration:

$$R_{\text{max}}(i) \sim \begin{cases} N^{2/5}\sigma^{-2/15} & \text{good solvent} \\ N^{1/3}\sigma^{-1/6} & \Theta \text{ solvent} \\ N^{1/4}\sigma^{-1/4} & \text{poor solvent} \end{cases} \quad (12)$$

Nonadsorbing particles with $R > R_{\text{max}}(i)$ are effectively expelled from the brush.

Overall the penetration into the interior of the brush is less favorable as the solvent quality improves. The opposite trend occurs at the outer edge of the brush because the steepness of the $\Pi(z)$ at the brush periphery increases as the solvent quality decreases. The poor solvent entries in eqs 8 and 10−12 are essentially identical to the ones obtained by Kim and O'Shaughnessy[6] for the case of a dry brush. Finally, the good solvent expressions are in semiquantitative agreement with the simulations results of Yaneva et al.[28] This molecular dynamics (MD) study simulated the penetration of spherical particles of radius R into a brush of moderately high σ swollen by a good solvent. The authors introduced a penetration length $\delta_o(R)$ defined as
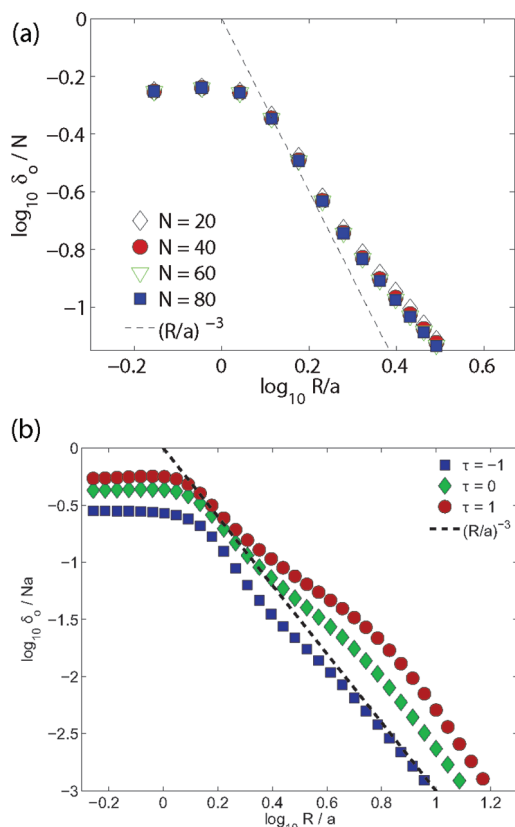
$$\delta_o(R) = \frac{\left[\int_0^\infty c_{\text{prt}}(z)\phi(z)\,\mathrm{d}z\right]^2}{\int_0^\infty c_{\text{prt}}^2(z)\phi^2(z)\,\mathrm{d}z} \quad (13)$$

measuring the overlap between the monomer and particle "clouds". The $\delta_o(R)$ thus defined does not require the determination of the brush height, H, and accordingly avoids difficulties in its identification from the simulation data. The plots of

(a)

(b)

(c)

$R = 5\,a$
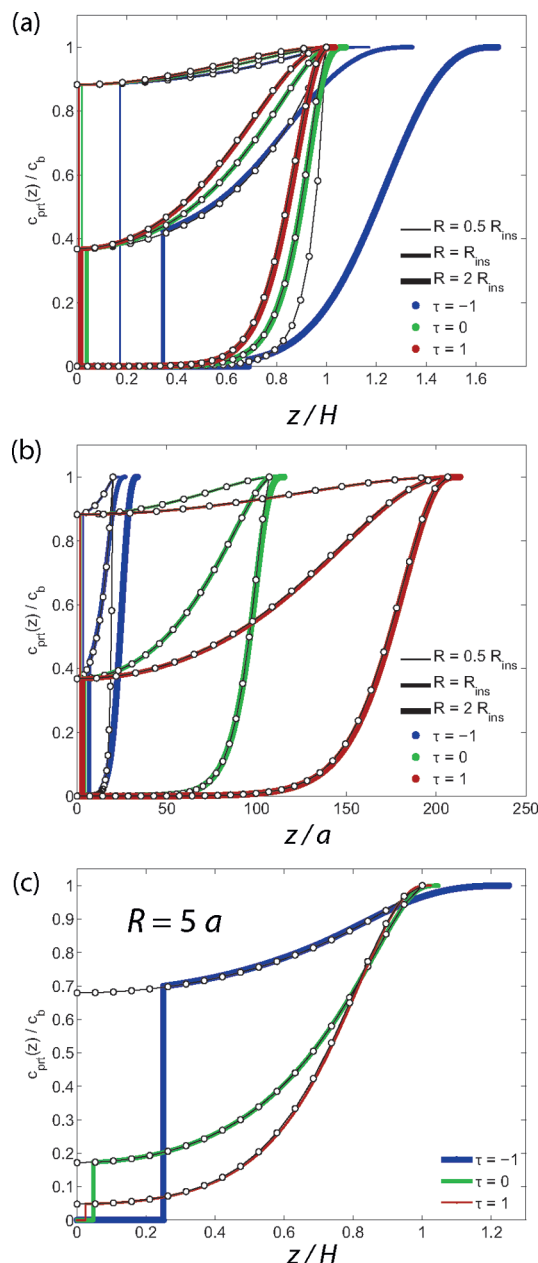
Figure 4. Plots of $c_{\text{prt}}(z)/c_b$ for penetration by non-adsorbing particles at $\tau = 1$, $\tau = 0$ and $\tau = -1$ for three different $R = 0.5 \times R_{\text{ins}}$, $R = R_{\text{ins}}$ and $R = 2 \times R_{\text{ins}}$ vs z/H (a) and vs z (b). For a fixed $R = 5a$ the $c_{\text{prt}}(z)/c_b$ vs z/H plots change with the solvent quality (c). The system parameters, $N = 1000$, $p = 1$, $a = 1$, $w = 1$, $\sigma = 0.01$ leading to $a \ll R \ll H$ in every case, are identical with those used to produce Figure 7a. Exact numerical solution of the SCF result (Appendix F) depicted by colored lines are compared to the results of eq 7 with the corresponding R_{ins} (black -o-o-o-). Deviations from the numerical SCF occur when (i) the $R \ll H$ condition is not fulfilled or (ii) at $z < R$ because 7 does not allow for hard core repulsion at the surface.

$\log_{10}\delta_o(R)/Na$ vs $\log_{10}R/a$ as calculated utilizing the SCF theory for the R and N values used by Yaneva et al.[28] are depicted in Figure 5. The SCF $\delta_o(R)/Na$ is essentially independent of N for the chosen τ and the R range considered. Indeed, in the analytical SCF theory addressing the $N \gg 1$ limit, $\delta_o(R)$ is strictly linear in N when $F_{\text{ins}}(z)$ is locally determined by $\Pi(z)$ (Appendix B). In contrast, the MD results indicate a certain N dependence. Yet,
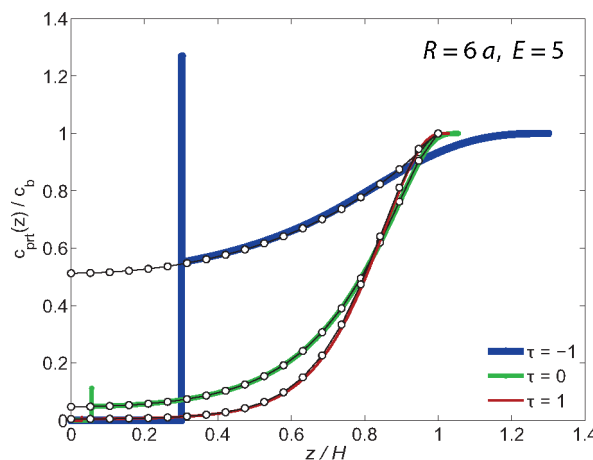
Figure 6. The combined effect of primary adsorption and penetration on $c_{prt}(z)$ for $\tau = +1$, 0, and -1 at $E = 5$. The primary adsorption gives rise to a spike with $c_{prim} = \Gamma_{prim}/R$. In the case depicted $R = 6a$ the adsorption scenario changes qualitatively with solvent quality since $R < R_{prim}$ under poor solvent conditions where $R_{prim} = 11.7a$ while in Θ and good solvent conditions, where $R_{prim} = 7.1a$ and $R_{prim} = 5.9a$, $R > R_{prim}$. In all three cases, $R > R_{ins}$ as seen from Figure 7a. obtained for identical system parameters. Exact numerical solutions of the SCF equations (Appendix F) depicted by colored lines are compared to eq 7 with the corresponding R_{ins} (black -o-o-o-).

Figure 5. (a) N dependence of the SCF $\log_{10}\delta_o(R)/Na$ (eq 13) vs $\log_{10}(R)/a$ curves for $\tau = 1$, and $N = 80, 60, 40, 20$, $\sigma = 0.185$, $w = 1$, and $p = 1$, leading to $\beta = 0.65$, $R_{ins} \approx 0.90$ and $H \approx 48.9a$, $36.7a$, $24.4a$, $12.2a$, respectively. The results are in semiquantitative agreement with the simulations results of Yaneva et al., cf. Figure 5a in ref 28. The $(R/a)^{-3}$ line is included to facilitate comparison with their data. (b) The effect of solvent quality on $\log_{10}\delta_o(R)/Na$ vs $\log_{10}R/a$ of brushes with $N = 80$ and solvents with $\tau = +1, 0, -1$, $\sigma = 0.185$, $w = 1$, and $p = 1$ leading to $\beta = +0.65, 0, -0.65$, $R_{ins} \approx 0.897a$, $0.96a$, $1.08a$, $H \approx 48.9a$, $36.8a$, $23.1a$, respectively. The penetration depth δ_o increases with increasing τ.

the agreement between the SCF and MD results is striking in both form and numerical values. It is especially notable in view of the poor performance of the analytical SCF theory at the exterior of finite brushes and three additional points: (i) the τ corresponding to the simulations is not specified precisely; (ii) the maximal $\phi(z)$ at the vicinity of the wall is high, $\phi(z) \approx 0.45$ thus suggesting that higher order virial terms may be necessary to accurately describe the system; (iii) one would expect $F_{ins} \approx \Pi_g(z)R^3$ to apply only to $R \gg a$.[52] It is also useful to note that the MD results are consistent with the insertion mode in that the $\phi(z)$ profiles were not affected by the nanoinclusions. Finally, notice that for all R the SCF $\delta_o(R)/N$ decreases with the solvent quality (Appendix B) reflecting the variation of brush height, H, and of the slope at the periphery of $\Pi(z)$. The effect of H dominates the behavior of small particles $R < R_{ins}$ exploring the whole brush, $0 < z < H$. The peripheral slope of $\Pi(z)$ dominates the behavior of the large particles expelled from the brush interior as manifested in $\delta_{ins}(i)$ discussed earlier.

IV. A BRIEF COMMENT ON PRIMARY ADSORPTION

Our preceding discussion concerned non-adsorbing particles whose interactions with both the wall and the polymer chains are

repulsive. The introduction of an attractive interaction favoring adsorption modifies the behavior of the system. A variety of adsorption modes are possible, differing with respect to the nature of the attractive free energy F_{att} driving the adsorption. In this section we comment on the case of pure primary adsorption, i.e., when the particles adsorb at the wall while the monomer-particle interactions are repulsive.[18,19,22,23] A simple model of this case invokes contact attraction to the surface such that a particle in grazing contact with the surface gains an adsorption energy $F_{att}/k_BT = -E \approx$ const'.[19,22,23] Our analytical results concern slowly varying $\Pi(z)$ such that $F_{ins}(z) \approx \Pi(z)R^3$. Accordingly, the free energy of an adsorbed particle at the wall is well approximated by $F_{prim} \approx -Ek_BT + \Pi_i(0)R^3$. Since adsorption is defined by grazing contact it is helpful to introduce a surface concentration $n = xn_{sat}$ where n_{sat} is the saturation value and $x \ll 1$ is the occupation fraction. Accordingly, $\mu_{ad} = F_{prim} + k_BT \ln x$ and the equilibrium adsorbed amount per unit area, as given by $\mu_{ad} = \mu_{bulk}$, is $\Gamma_{prim} = n = c_b n_{sat} \exp(-F_{prim}/k_BT)$. Consequently, lowering solvent quality for a given R favors adsorption because $\Pi_p(0) < \Pi_\Theta(0) < \Pi_g(0)$. The onset of primary adsorption is specified by the condition $F_{prim} = 0$ defining a characteristic R_{prim}. For Θ solvents and the asymptotic regimes, it yields

$$R_{prim}(i) \approx \left[\frac{Ek_BT}{\Pi_i(0)}\right]^{1/3} = E^{1/3}R_{ins}(i) \qquad (14)$$

such that particles adsorb when $R < R_{prim}(i)$. The adsorption of larger particles $R > R_{prim}(i)$, is repressed because F_{ins} overcomes F_{att}. Primary adsorption is only significant when $E > 1$ and thus $R_{prim}(i) > R_{ins}(i)$. It is accordingly helpful to distinguish three situations: (i) $R \gg R_{prim}(i) > R_{ins}(i)$ when primary adsorption is repressed and the particles are largely expelled from the brush, (ii) $R_{prim}(i) > R \gg R_{ins}(i)$ when primary adsorption at the surface occurs while particle penetration is limited to the outer edge of the brush, and (iii) $R_{prim}(i) > R_{ins}(i) > R$ when the particles both

penetrate the brush and adsorb at the wall. When primary adsorption plays a role, in cases ii and iii, the overall concentration profile is a superposition of the "penetration" $c_{prt}(z) < c_b$ given by eq 7 and a spike at $z = R$ accounting for adsorption at the wall. The spike defines an adsorbed layer of thickness $\sim R$ and concentration $c_{prim} \approx \Gamma_{prim}/R$ which may exceed c_b. Since $R_{ins}(p) > R_{ins}(\Theta) > R_{ins}(g)$, varying the solvent quality may result in a change of the adsorption behavior of a particle of given R (Figure 6).

In the simple model described above $F_{att} = -Ek_BT$ for a particle at grazing contact and F_{att} exhibits no R dependence. It is useful to note two effects contributing to deviations from this scenario. The SCF $\phi(z)$ profiles are monotonically decreasing with a maximum at $z = 0$. In reality, $\phi(z)$ exhibits a minimum at the wall. In turn, inserted particles can thus experience a "depletion" attraction at the vicinity of $z = 0$,[25] an effect that depends on R. Second, an R dependence can also arise if the wall is penetrable as can be the case for lamellar phases of block copolymers. In addition, E in our simplified discussion is independent of T. This approximation may fail when the τ range explored is wide. Finally, note that primary adsorption is an activation process and requires overcoming a free energy barrier $\approx F_{ins}(0)$.[22]

V. TERNARY ADSORPTION WITHIN THE BRUSH DUE TO WEAK PARTICLE MONOMER ATTRACTION

As noted earlier, the adsorption behavior depends on the characteristics of the free energy driving it, F_{att}. Here we focus on the case of pure ternary adsorption arising because of weak non-specific monomer-particle attraction.[20,23,24] In this scenario the surface of the particle is assumed to be uniform and a monomer at grazing contact with the particle is assigned an energy of $-\varepsilon k_BT$ with $0 < \varepsilon \ll 1$ to ensure that there is no distortion of the brush concentration profile.[47] This last requirement is necessary to justify the assumption of an insertive mode and the applicability of eq 1. For simplicity, we ignore the T dependence of ε noting that it may play a role if the τ range is wide. For brevity, we consider again spherical particles with $R \ll H_i$. In this case, $\phi(z)$ experienced by the particle is roughly constant and approximated by its unperturbed value at the particle's center of mass. Consequently, the penalty incurred by a single fully inserted particle at z, $F_{ins}(z) \approx \Pi_i(z)R^3$, is opposed by attractive term $F_{att}(z)/k_BT \approx -\varepsilon\phi(z)(R/a)^2$, where $\phi(z)/a^3$ is the monomer concentration at z. For Θ solvents and the asymptotic regimes, $F_{att}(z)$ is

$$\frac{F_{att}(z)}{k_BT} = -\varepsilon\left(\frac{R}{a}\right)^2\phi_i(0)u^{n_i}(z/H_i) \quad (15)$$

where $n_g = 1$, $n_\Theta = 1/2$, and $n_p = 0$. Here we ignore the higher order correction to $\phi_p(z)$ which is crucial for the determination of $\Pi_p(z)$ but has negligible effect on $F_{att}(z)$,[53] i.e., $\phi_p(0) = \overline{\phi}_p$. Note that this F_{att} applies to solvent swollen brushes where $\phi_p(z) < 1$ varies with z and not to dry brushes.

In contrast to primary adsorption at the wall, ternary adsorption is driven by a z-dependent $F_{att}(z)$. This introduces additional length scales supplementing $R_{ins}(i)$. Two are especially useful. The first, analogous to $R_{ins}(i)$, characterizes $F_{att}(z)$. As for ternary adsorption, $F_{att}(z) \sim R^2$, the particle must exceed a certain R in order to attain $F_{att}(z) < -k_BT$. Since $F_{att}(z) \sim \phi(z)$ and the SCF $\phi(z)$ is monotonically decreasing it is helpful to introduce R_{att} via the condition $F_{att}(0)/k_BT \approx -\varepsilon\phi(0)(R/a)^2 \approx -1$. While the range

$0 \leq z < R$ is physically inaccessible, $F_{att}(0)$ sets the scale of $F_{att}(z)$. For the asymptotic and Θ regimes $F_{att}(0) \approx -k_BT$ yields

$$R_{att}(i) \approx \frac{a}{\sqrt{\varepsilon\phi_i(0)}} \sim \begin{cases} \tau^{1/6}\varepsilon^{-1/2}\sigma^{-1/3} & \text{good solvent} \\ \varepsilon^{-1/2}\sigma^{-1/4} & \Theta \text{ solvent} \\ |\tau|^{-1/2}\varepsilon^{-1/2} & \text{poor solvent} \end{cases}$$

$$(16)$$

When $R < R_{att}(i)$ the particle does not reach $F_{att}(z) < -k_BT$ at any z while in the opposite case it attains $F_{att}(z) < -k_BT$ at a certain z range. Since $F_{att}(z) \sim \phi(z)$ and the brush density grows upon decreasing solvent quality $R_{att}(g) < R_{att}(\Theta) < R_{att}(p)$ i.e., ternary adsorption is favored by lower solvent quality. The free energy of a particle undergoing weak ternary adsorption, $F_{tern} = F_{ins} + F_{att}$, as expressed in terms of $R_{ins}(i)$ and $R_{att}(i)$, is

$$\frac{F_{tern}(z)}{k_BT} \approx -\left[\frac{R}{R_{att}(i)}\right]^2 u^{n_i}(z/H_i) + \left[\frac{R}{R_{ins}(i)}\right]^3 u^{m_i}(z/H_i) \quad (17)$$

where $m_g = 2$, $m_\Theta = 3/2$, $m_p = 1$.[53] To discuss the particle concentration profiles it is helpful to consider a crossover altitude z_{co} where the two opposing contributions cancel and $F_{tern}(z_{co}) = 0$. This condition amounts to $u^{m_i-n_i}(z_{co}/H_i) = R_{ins}^3(i)/R_{att}^2(i)R \equiv R_{co}(i)/R$ where $R_{co}(i)$ corresponds $F_{tern}(0) = 0$. Since $m_i - n_i = 1$ for the three solvent regimes

$$\frac{z_{co}(i)}{H_i} = \sqrt{1 - \frac{R_{co}(i)}{R}} \quad (18)$$

where

$$R_{co}(i) = R_{ins}^3(i)/R_{att}^2(i) \sim \begin{cases} \varepsilon\tau^{-2/3}\sigma^{-2/3} & \text{good solvent} \\ \varepsilon\sigma^{-1} & \Theta \text{ solvent} \\ \varepsilon|\tau|^2\sigma^{-2} & \text{poor solvent} \end{cases}$$

$$(19)$$

and $R_{co}(p) > R_{co}(\Theta) > R_{co}(g)$. The role of $R_{co}(i)$ for ternary adsorption is similar to the role of $R_{ins}(i)$ in the penetration scenario. When $R > R_{co}(i)$ ternary adsorption can occur only at $z_{co} < z < H_i$. For $R < R_{co}(i)$ the particles may adsorb throughout the brush.

Overall, ternary adsorption is negligible when $R < R_{att}(i)$ and $F_{att} > -k_BT$ throughout the brush. When $R > R_{att}(i)$ it is helpful to distinguish between two cases (Figure 7): ternary adsorption is high and occurs at any $0 < z < H_i$ when $R_{att}(i) < R < R_{co}(i)$. On the other hand, for $R > R_{att}(i)$ and $R > R_{co}(i)$, the adsorption is lower and it shifts to the brush periphery. In every regime, it grows with R. Since ternary adsorption is significant when $R_{att}(i) < R < R_{co}(i)$, it is helpful to consider the width of the relevant R range as characterized by

$$\frac{R_{co}(i)}{R_{att}(i)} \sim \varepsilon^{3/2} \begin{cases} \tau^{-5/6}\sigma^{-1/3} & \text{good solvent} \\ \sigma^{-3/4} & \Theta \text{ solvent} \\ |\tau|^{5/2}\sigma^{-2} & \text{poor solvent} \end{cases} \quad (20)$$

The inequality $R_{co}(i) > R_{att}(i)$ is realized when $\varepsilon > \tau^{5/9}\sigma^{3/2}$ for good solvent, $\varepsilon > \sigma^{1/2}$ for Θ solvent, and $\varepsilon > |\tau|^{-5/3}\sigma^{3/2}$ for poor solvent. Accordingly, ternary adsorption is significant in poor solvents where $R_{co}(i) > R_{att}(i)$ is easily attainable for $\varepsilon \ll 1$. In contrast, the adsorption range is very narrow in Θ and
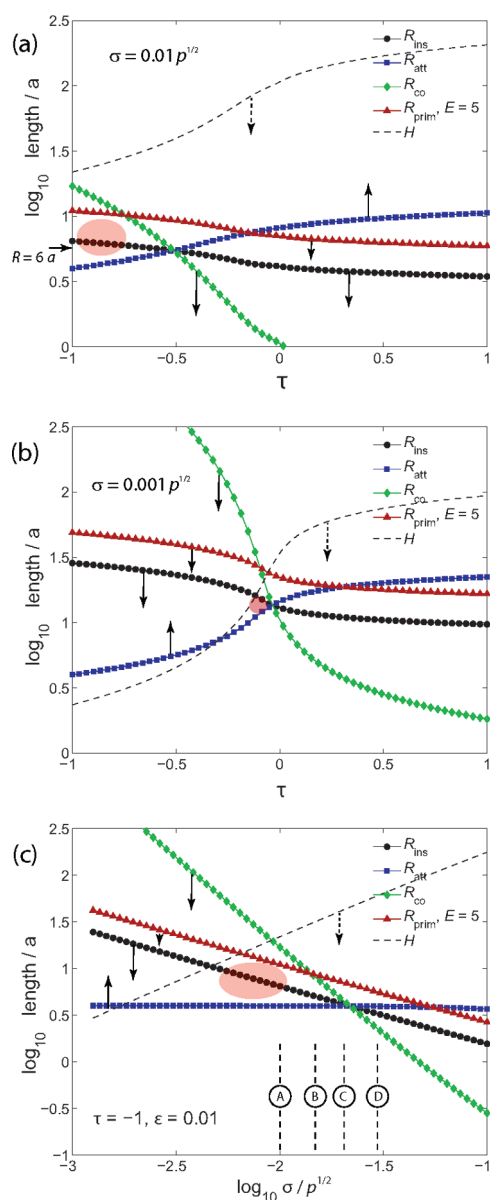
Figure 7. Penetration and adsorption regimes determined by the relative magnitude of the characteristic lengths: R_{ins}, R_{att}, R_{co}, and R_{prim} as defined in Appendix F, and the brush height, H. (a, b) The logarithmic variation of these lengths with τ and with $\log \sigma/p^{1/2}$ delineates the different brush regimes. Penetration of a sphere of radius R is significant when $R < R_{ins}$, primary adsorption is important when $R < R_{prim}$, and ternary adsorption is appreciable when $R_{att} < R < R_{co} < H$. This last regime, depicted by a red ellipsoid, is attainable in poor solvents but difficult to realize in Θ and good solvents as seen from plots of R_{co}, R_{att} and H vs τ for (a) $\sigma = 0.01$ and (b) $\sigma = 0.001$. (c) Effect of surface density σ on the characteristic lengths in the poor solvent case with $\tau = -1$, where significant ternary adsorption can occu. In all cases $N = 1000$, $w = 1$, $p = 1$, and $\varepsilon = 0.01$. The four systems (A–D), defined in part c, are investigated in more detail in Figure 8.

good solvents (Figure 8). Within this picture, ternary adsorption of spherical particles is appreciable only in poor solvents. Note however that this conclusion may change for aspherical particles with higher ratio of surface area to volume.[23] This picture is quantified by the explicit $c_{prt}(z)$ when expressed in terms of $R_{co}(i)$ and $R_{att}(i)$. At equilibrium, $\mu_{bulk} = \mu(z)$ with
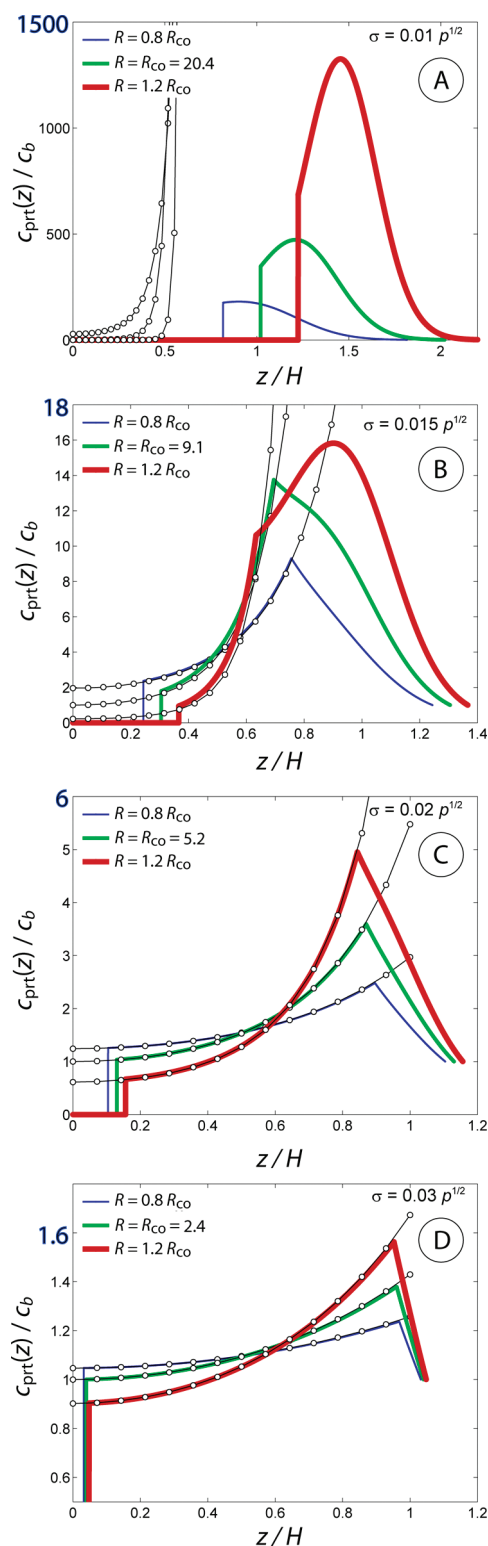
Figure 8. $c_{prt}(z)/c_b$ vs z/H for pure ternary adsorption within classical brushes immersed in poor solvent with $R = 0.8 \times R_{co}$, $R = R_{co}$, $R = 1.2 \times R_{co}$, obtained for the parameter sets A–D in Figure 7c, i.e., at surface densities (A) $\sigma = 0.01$, (B) $\sigma = 0.015$, (C) $\sigma = 0.02$, and (D) $\sigma = 0.03$. Under Θ and good solvent conditions $R_{co} < a$ is the typical scenario, cf. Figure 7a, and thus not illustrated. Exact numerical solutions of the SCF equations (Appendix F) depicted by colored lines are compared to the results of eq 21 with the corresponding R_{att} and R_{co} (black -o-o-o-). Deviations are important when $R \ll H$ is not realized.

$\mu(z) = k_B T \ln c_{prt}(z) + F_{tern}(z)$ thus leading to $c_{prt}(z) = c_b \exp(-F_{tern}(z)/k_B T)$ or

$$\frac{c_{prt}(z)}{c_b}$$

$$= \begin{cases} \exp\left\{\left[\frac{R}{R_{att}(g)}\right]^2\left[u_g - \frac{R}{R_{co}(g)}u_g^2\right]\right\} \text{good solvent} \\ \exp\left\{\left[\frac{R}{R_{att}(\Theta)}\right]^2\left[u_\Theta^{1/2} - \frac{R}{R_{co}(\Theta)}u_\Theta^{3/2}\right]\right\} \Theta \text{ solvent} \\ \exp\left\{\left[\frac{R}{R_{att}(p)}\right]^2\left[1 - \frac{R}{R_{co}(p)}u_p\right]\right\} \text{poor solvent} \end{cases} \quad (21)$$

where u_i abbreviates $u(z/H_i)$. Equation 21 underlines an additional effect of the solvent quality on the SCF $c_{prt}(z)$: In poor solvent $F_{att}(z) \approx const'$ and $c_{prt}(z)$ of a fully inserted particles is monotonically increasing (Figure 8) because $F_{int}(z)$ is monotonically decreasing. On the other hand, in good and Θ solvents $c_{prt}(z)$ can exhibit a maximum at $0 < z < H_i$ reflecting the interplay of $F_{att}(z)$ and $F_{int}(z)$. Increasing R causes the maximum to shift outward and increases the maximal value of $c_{prt}(z)$ (Appendix C). Our analytical results do not allow for partial insertion at the edge of the brush. As a result the poor solvent $c_{prt}(z)$ exhibits a jump at the brush edge with $c_{prt}(H_p) > c_b$. This artifact that does not occur for the exact numerical solution (Appendix D). As in the penetration case, our results assume an especially simple form in the limit of $R \gg R_{co}(i)$. These expressions are subject to the same reservations discussed in section III. For comparison purposes they are listed in Appendix D.

The adsorption isotherm, specifying the total adsorbed amount per unit area corresponding to $c_{prt}(z)$ is

$$\Gamma = \int_0^H c_{prt}(z)\, dz \quad (22)$$

Note that this Γ measures only the contribution of fully inserted particles. To allow for partially inserted ones the upper limit of the integral should be extended to $H + R$, a correction of negligible effect when $R \ll H$. For poor solvents with $\beta \ll -1$, when ternary adsorption is pronounced, Γ is

$$\Gamma_p = \frac{\pi^{1/2}}{2} c_b H_p \left[\frac{R_{ins}(p)}{R}\right]^{3/2} \exp\left[\left(\frac{R}{R_{att}(p)}\right)^2\left(1 - \frac{R}{R_{co}(p)}\right)\right]$$

$$\times \text{erfi}\sqrt{\frac{R^3}{R_{ins}^3(p)}} \quad (23)$$

where $\text{erfi}(z) = \text{erf}(iz)/i$ is the imaginary error function such that $\text{erfi}(x) = 2x(3 + x^2)/3\pi^{1/2}$ for $x \ll 1$ and $\text{erfi}(x) = \pi^{-1/2}x^{-1}\exp x^2$ for $x \gg 1$. Γ exhibits a maximum at $R \approx R_{ins}(p)$ reflecting the interplay between $F_{att} \sim R^2$ favoring adsorption and $F_{ins} \sim R^3$ opposing it. The good solvent case Γ_g was already studied focusing on the σ dependence for a fixed R.[24] Overall, poor solvent favors the adsorption of large particles with $R_{att} \ll R \ll R_{co}$ while Γ of small particles with $R < R_{ins}$ and $R < R_{att}$ increases with H and the solvent quality because they explore the whole $0 < z < H$ range (Figure 9 and Appendix E).
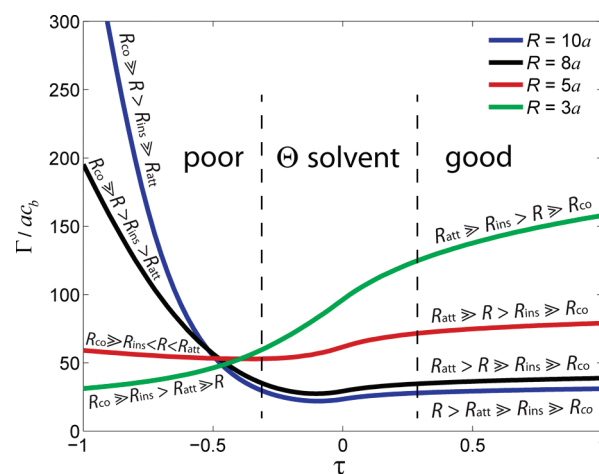
Figure 9. Γ/ac_b vs τ for pure ternary adsorption of spherical particles within classical brushes as obtained for radii $R = 3a$, $R = 5a$, $R = 8a$, and $R = 10a$. For the parameters utilized, as in Figure 7a, R as well as R_{ins} and R_{att} are small compared with H under all solvent conditions. In the interval $-1 \le \tau \le 1$ the characteristic dimensions vary in the range $R_{ins}/a = 6.9 - 3.5$, $R_{att}/a = 4.0 - 10.6$, $H/a = 20 - 206$. Poor solvents favor the adsorption of larger particles while penetraion of small particles, exploring the full depth of the brush, is favored by good solvents.

VI. DISCUSSION

Solvent quality affects the interactions between polymer brushes and colloidal particles. Our discussion of these effects focused on the "insertion limit" when a particle inside the brush induces only short ranged perturbation of the monomer concentration profile. For spherical particles this is the case when $R \ll H$ and the particle-monomer interactions are repulsive or weakly attractive. In this situation, a particle placed at altitude z incurs a free energy penalty $F_{ins}(z) \approx \Pi(z)R^3$ related to the work against the osmotic pressure $\Pi(z)$ in the unperturbed brush. $\Pi(z)$ is the osmotic pressure in a bulk polymer solution of $\phi = \phi(z)$. Our SCF analysis focused on "classical brushes" whose behavior in all solvent regimes is described by an interaction free energy density $f_{int}[\phi(z)]a^3 = \tau\phi^2(z) + w\phi^3(z)$, as realized in non-aqueous solvents. Since our discussion concerns the role of $F_{ins}(z) \approx \Pi(z)R^3$ and its variation with solvent quality it requires knowledge of the corresponding SCF $\Pi(z)$ profiles. Obtaining the $\Pi(z)$ profiles for good and Θ solvents is straightforward. However, in the poor solvent limit the analytical form of the SCF $\phi(z)$ must allow for a second order term to obtain the correct $\Pi(z)$ of the collapsed brush. In particular

$$\frac{\phi(z)}{\phi_p} = 1 + const'\left(1 - \frac{z^2}{H_p^2}\right) \quad (24)$$

for $\beta \ll -1$ thus leading to

$$\frac{\Pi_p(z)}{\Pi_p(0)} = 1 - \frac{z^2}{H_p^2} \quad (25)$$

where $\Pi_p(0)a^3/k_B T \sim \sigma^2/p\phi_p(0)$. Neglecting the second order term in $\phi(z)$ would yield $\Pi_p(z) = 0$.

In every case considered the particle concentration profile $c_{prt}(z) \sim \exp[-F_{ins}(z)/k_B T]$ is strongly dependent on R because $F_{ins}(z) \approx \Pi(z)R^3$. Accordingly, larger R always favor expulsion irrespective of the solvent quality. For a given R, the "expulsion tendency" increases with the solvent quality since $\Pi_g(0) >$

$\Pi_{\Theta}(0) > \Pi_p(0)$. However, the definition of "large" and "small" R depends on both solvent quality and particle interactions. In the penetration scenario, when the particles are non-adsorbing, $c_{prt}(z) < c_b$ is monotonically increasing with z. In this case, the yardstick for R is $R_{ins}(i) \approx (k_B T/\Pi_i(0))^{1/3}$ and expulsion is significant for $R > R_{ins}(i)$. In turn, $R_{ins}(i)$ increases with osmotic pressure and thus with the solvent quality: $R_{ins}(p) \sim \sigma^{-2/3} > R_{ins}(\Theta) \sim \sigma^{-1/2} > R_{ins}(g) \sim \sigma^{-4/9}$. To illustrate the effect of solvent quality note that particles of size $R_{ins}(\Theta) \ll R < R_{ins}(p)$ will penetrate the interior of a collapsed brush but will be expelled from brushes swollen by Θ or good solvents. An additional length scale emerges when particle–wall attraction plays a role. Our discussion focused on the simplest case of primary adsorption at the wall when the particle–wall contact free energy $-Ek_BT$, and E does not vary with R or T. In this case $R_{ins}(i)$ is supplemented by $R_{prim}(i) \approx E^{1/3}R_{ins}(i)$ such that primary adsorption occurs when $R < R_{prim}$. Accordingly, in choosing R to control $c_{prt}(z)$, it is important to take both $R_{ins}(i)$ and $R_{prim}(i)$ into account. For example, when $R_{prim} \gg R \gg R_{ins}(i)$ the particles adsorb at the wall while being largely depleted from most of the brush interior. Note that in this case, as opposed to the penetration scenario, the particle concentration at the wall, $c_{prim} \approx \Gamma_{prim}/R$, can exceed c_b. Allowing for monomer–particle attraction introduces new length scales. Our discussion focused on the weak ternary adsorption where a monomer at contact with the surface gains $-\varepsilon k_BT$ with $0 < \varepsilon \ll 1$ thus leading to $F_{att}/k_BT \approx -\varepsilon R^2\phi(z)/a^2$. Very small particles are not affected because $F_{att} \sim R^2$. To accumulate $F_{att} < -k_BT$ the particle should be larger than $R_{att}(i)$ where $R_{att}(g) \sim a\varepsilon^{-1/2}\sigma^{-1/3} > R_{att}(\Theta) \sim a\varepsilon^{-1/2}\sigma^{-1/4} > R_{att}(p) \sim a\varepsilon^{-1/2}$. On the other hand $F_{ins} \sim R^3$ eventually dominates at large R. The onset of this last effect occurs at $R > R_{co}(i) = R_{ins}^3(i)/R_{att}^2(i)$ where $R_{co}(g) \sim \varepsilon a/\sigma^2 > R_{co}(\Theta) \sim \varepsilon a/\sigma > R_{co}(g) \sim \varepsilon a/\sigma^{2/3}$. For $R_{att}(i) < R < R_{co}(i)$, ternary adsorption occurs throughout the brush and $c_{prt}(z) > c_b$ is proportional to $\phi(z)$. For spherical particles this regime is easily fulfilled only in poor solvents. Particles with $R > R_{co}(i)$ are depleted from the brush interior and their $c_{prt}(z)$ exhibits a maximum. When ternary adsorption is operative expulsion from the layer occurs for $R \gg R_{co}(i)$ rather than for $R \gg R_{ins}(i)$.

For comparison with experiments and simulations it is important to note the limitations of the theory. The analytical SCF theory we utilize does not describe depletion at the wall nor fluctuation effects at the edge. It translates bulk binodals into sharp boundaries rather than into diffuse interfaces. Thus, the outer boundary of collapsed brush is associated with a sharp jump in $\phi(z)$ rather than gradual variation. Overall, the theory overestimates F_{ins} at the wall while underestimating its outer range. Since the analytical form of the SCF theory utilizes $f_{int}[\phi(z)]a^3 = \tau\phi^2(z) + w\phi(z)^3$ it is applicable only when $\phi(z)$ is sufficiently low and higher virial terms are negligible. As implemented it focuses on uniform and monodispersed brushes grafted onto planar surfaces. It does not allow for polydispersity in N and Σ nor for surface roughness. While eq 1 allows to specify F_{ins} of particles of different forms our discussion concerned spherical particles with uniform surfaces. It is important to note that ternary adsorption is sensitive to shape, and aspherical particles may exhibit distinctive features. With these caveats, the theory provides guidelines on tuning brush–colloid interactions and, in particular, the interplay of R and σ.

The effect of solvent quality on particle–brush interactions is best documented in the case of thermoresponsive PNIPAM brushes and proteins. Collapsed PNIPAM brushes adsorb proteins much more than swollen ones.[15−17] While NWSP brushes undergoing collapse in water are beyond the scope of our theory, this is an important example of the role of solvent quality in tuning interactions. Similar effects for organic solvents were studied using evanescent wave dynamic light scattering measurements to probe particle penetration into brushes and demonstrated size and solvent quality dependence.[54] The qualitative aspects of the adsorption scenarios we considered are supported by two types of experiments. One concerns protein adsorption onto NWSP brushes. It involves studies of the adsorption isotherms $\Gamma(\Sigma)$ and the adsorption modes were deduced from their Σ dependence[19,21,23] because direct characterization of protein $c_{prt}(z)$ is difficult. The observation that $\Gamma(\Sigma)$ increases with Σ for $N \lesssim 200$ supports primary adsorption and is consistent with $\Gamma_{prim} \sim \exp(-F_{prim}/k_BT)$. The ternary adsorption scenario rationalizes the observation of a maximum in $\Gamma(\Sigma)$ for $N \lesssim 700$. The second group of experiments involves inorganic colloids where $c_{prt}(z)$ can be probed directly using electron microscopy,[55,56] X-ray[57] and neutron reflectometry.[8] A study involving a melt planar brush suggested expulsion[57] as discussed by Kim and O'Shaughnessy.[6] This case is closest to our discussion because Σ is not affected by the colloidal particles. Three different scenarios were observed when nano particles are incorporated into lamellar phases of AB diblock copolymers: (i) localization in the middle of the A phase suggestive of penetration and strong expulsion as considered in section III;[8,56] (ii) uniform distribution in the A phase suggestive of penetration with weak expulsion;[55] (iii) localization at the AB boundary of the AB diblock copolymer lamellar phase, corresponding to primary adsorption discussed in section IV.[8,55] The particle distribution was tuned by change in colloid size[8] surface chemistry[55] or lamellar domain size.[56] A theoretical discussion of these systems should allow for the possible modification of the diblock copolymers' phase behavior by the particles.[9,10,58] It is useful to note that the production of such composites involves solutions and in certain cases the final state is partially swollen.[56] Accordingly, ternary adsorption, as discussed above, may play a role in such systems.

Computer simulations afford the potential for detailed confrontation with theory. Thus, far simulations of colloids interacting with solvent swollen brushes focused exclusively on the good solvent regime. Within them one may discern two directions. One concerns studying the insertion of a single particle into a brush. It provides evidence for the insertion mode with local perturbation of the monomer concentration profile and its regime of applicability.[25,27,28,30] It also allows to measure to the insertion free energy thus confirming eq 1.[25,29,30] In the second direction the simulations model a brush interacting with many colloidal particles and allow to monitor the particle concentration profile.[28,51] These simulations confirm again the applicability of the insertion mode. The expulsion of larger particles is also evident. Detailed comparison with SCF theory is however difficult because the currently explored R range is narrow and close to $R_{ins}(g)$. Additional problems arise because the distal $\phi(z)$ of finite brushes deviates from the analytical SCF theory predictions. The comparison is also hampered by difficulties in determining the brush height, which then translate into uncertainties in quantifying particle penetration into the brush. In spite of this difficulties the SCF results are in semiquantitative agreement with the MD simulations of Yaneva et al.[28] (Figure 5). Brush–particles interactions in Θ and poor solvents are yet to be explored.

■ APPENDIX A: ASCF

The aim of this Appendix is to summarize the methods of (i) obtaining explicit $\phi(z)$ for semidilute classical brushes described by $f_{int}a^3 = \tau\phi^2(z) + w\phi^3(z)$ with extended analysis of collapsed brushes and the Θ region and (ii) obtaining the corresponding $\Pi(z)$ from the elastic free energy density f_{el} and demonstrating balance of the local osmotic pressure $\Pi(z)a^3/k_BT = \tau\phi^2(z) + 2w\phi^3(z)$ with the average tension per unit area. Within this version of the SCF theory,[37] the free energy per chain in the brush is

$$\frac{F_{chain}}{k_BT} = \frac{F_{el}}{k_BT} + \frac{F_{int}}{k_BT}$$

$$= \frac{3}{2pa^2}\int_0^H dh\, g(h)\int_0^h E(h,z)\, dz + \Sigma\int_0^H f_{int}[\phi(z)]\, dz$$

(A1)

The first term allows for the elastic free energy while the second reflects the contribution due to monomer−monomer interactions. In the elastic free energy the length $E(h,z) = dz/dn$ is proportional to the local tension at z when the chain end is at h, $(3k_BT/pa^2)E(h,z)$, and n specifies the position of the monomer along the contour of the chain. $g(h)$ is the distribution function of the altitude of the free ends, h. The average tension per unit area at altitude z, $T_n(z)$, is thus

$$T_n(z) = \frac{3k_BT}{pa^2\Sigma}\int_z^H E(h,z)g(h)\, dh$$

(A2)

The interaction free energy giving rise to the second term is specified in terms of the free energy density $k_BTf_{int}[\phi(z)]$. In the strong stretching approximation, only chains with $h \geq z$ contribute to $\phi(z)$ and the three unknown functions specifying the brush are related via

$$\phi(z) = \frac{a^3}{\Sigma}\int_z^H \frac{g(h)}{E(h,z)}\, dh$$

(A3)

The brush properties are determined by minimization of F_{chain} subject to two constraints

$$\int_0^h \frac{dz}{E(h,z)} = N$$

(A4)

and

$$\frac{\Sigma}{a^3}\int_0^H \phi(z)\, dz = N$$

(A5)

The minimization leads to two key equations

$$E(h,z) = \frac{\pi}{2N}\sqrt{h^2 - z^2}$$

(A6)

and

$$\frac{a^3\partial f_{int}}{\partial\phi} \equiv U(z) = \Lambda - \frac{3\pi^2}{8pa^2N^2}z^2$$

(A7)

Once Λ is determined via the constraint A5, this last equation yields explicit solutions for $\phi(z)$ when $U(z) = 2\tau\phi^2 + 3w\phi^2$. We first utilize eqs A6 and A7 to obtain an explicit expression for $\Pi(z)$ in terms of $\phi(z)$ for the yet unknown Λ. Importantly, the resulting expression for $\Pi(z)$ is valid for arbitrary f_{int}. To this end we introduce an elastic free energy density $k_BTf_{el}(z)$ such that

$F_{el} = k_BT\Sigma\int_0^H f_{el}(z)\, dz$ or

$$f_{el}(z) = \frac{3}{2pa^2\Sigma}\int_z^H E(h,z)g(h)\, dh$$

$$= \frac{3\pi}{4Npa^2\Sigma}\int_z^H \sqrt{h^2 - z^2}g(h)\, dh = \frac{T_n(z)}{2k_BT}$$

(A8)

To express $f_{el}(z)$ as a function of $\phi(z)$ and z we first consider

$$\frac{df_{el}}{dz} = -\frac{3\pi}{4Npa^2\Sigma}z\int_z^H \frac{g(h)}{\sqrt{h^2 - z^2}}\, dh = -\frac{3\pi^2}{8N^2pa^5}z\phi(z)$$

(A9)

thus leading to

$$f_{el}(z) = -\int_z^H \frac{df_{el}}{dz}\, dz = \frac{3\pi^2}{8N^2pa^5}\int_z^H t\phi(t)\, dt$$

(A10)

which recovers A9 upon taking the derivative and satisfies the requirement that $f_{el} = 0$ at $z = H$. Noting the similarity between the RHS of eq A10 and dU/dz as given by eq A7, together with $U(z) = a^3\partial f_{int}/\partial\phi$ and $\int_z^H U(z)\, d\phi = \int_z^H df_{int}$ leads to

$$f_{el}(z)a^3 = -\frac{1}{2}\int_z^H \frac{dU(t)}{dt}\phi(t)\, dt = \frac{1}{2}U(z)\phi(z)$$

$$-\frac{1}{2}U(H)\phi(H) + \frac{1}{2}\int_z^H U(z)\, d\phi(t) = \frac{\Pi(z)a^3}{2k_BT} - \frac{\Pi(H)a^3}{2k_BT}$$

(A11)

For a free brush at equilibrium, when $\Pi(H) = 0$, this ensures the local force balance, $\Pi(z) = T_n(z)$ and specifies the local osmotic pressure within the SCF theory $\Pi(z)/k_BT = 2f_{el}(z)$. One may thus calculate $\Pi(z)$ utilizing eq A10 or $\Pi(z)a^3/k_BT = \tau\phi^2(z) + 2w\phi^3(z)$.

The Concentration Profile. Equation A7 yields an explicit expression for $\phi(z)$ in the particular case of $f_{int}a^3 = \tau\phi^2(z) + w\phi^3(z)$ and $U(z) = 2\tau\phi + 3w\phi^2$. In this case A7 is a quadratic equation in ϕ solved by

$$\phi(z) = \frac{-\tau + \sqrt{\tau^2 + 3w\left(\Lambda + \frac{3\pi^2}{8pN^2a^2}z^2\right)}}{3w}$$

(A12)

where the volume fraction at the outer edge of the brush, $z = H$, is $\phi(H) = 0$ for $\tau \geq 0$ while for $\tau < 0$ it is $\phi(H) = \overline{\phi}_p = |\tau|/2w$. It is convenient to discuss the general case in terms of the solution at the Θ temperature where $\tau = 0$ and the condition $\phi(H) = 0$ together with the constraint A5 leads to $\phi(z) = \phi_\Theta u^{1/2}$ as specified by Table 1. Allowing for the appropriate $\phi(H)$ and upon introducing β, eq 3, and the swelling ratio $\alpha(\beta) \equiv H(\beta)/H_\Theta$, enable to express eq A12 as

$$\phi(z) = \begin{cases} \frac{\tau}{3w}\left[\sqrt{1 + \beta^{-2}(\alpha^2 - y^2)} - 1\right] & \beta \geq 0 \\ \frac{|\tau|}{3w}\left[\sqrt{\frac{1}{4} + \beta^{-2}(\alpha^2 - y^2)} + 1\right] & \beta < 0 \end{cases}$$

(A13)

where $y \equiv z/H_\Theta$. The constraint A5 leads, upon noting that $(3w/\tau)(Na^3/\Sigma H_\Theta) = \pi/4\beta$ and $\arctan t = \arcsin t(1 + t^2)^{-1/2}$, to

$$\frac{\pi}{2\beta^2} = \begin{cases} -\dfrac{\alpha}{\beta} + \left(1 + \dfrac{\alpha^2}{\beta^2}\right) \arcsin \dfrac{\alpha}{\sqrt{\alpha^2 + \beta^2}} & \beta \geq 0 \\[4mm] -\dfrac{5}{2}\dfrac{\alpha}{\beta} + \left(\dfrac{1}{4} + \dfrac{\alpha^2}{\beta^2}\right) \arcsin \dfrac{\alpha}{\sqrt{\alpha^2 + \beta^2/4}} & \beta < 0 \end{cases}$$
$$(A14)$$

In turn, eq A14 yields simple expressions for $\alpha = \alpha(\beta)$ in three limits. Two correspond to $|\beta| \gg 1$, when $\alpha \ll |\beta|$ thus allowing to invoke $\arctan t \approx t - t^3/3$. The third concerns the vicinity of the Θ point, when $\alpha \approx 1$ and $\beta \approx 0$, $\alpha = 1 + \beta(d\alpha/d\beta)_{\beta = 0}$ with $(d\alpha/d\beta)_{\beta = 0} = 2/\pi$. Altogether

$$\alpha(\beta) = \begin{cases} \left(\dfrac{3\pi}{4}\right)^{1/3} \beta^{1/3} & \text{good solvent,} & \beta \gg 1 \\[3mm] 1 + \dfrac{2}{\pi}\beta & \text{near } \Theta \text{ solvent,} & \beta \ll 1 \\[3mm] \dfrac{\pi}{6|\beta|} & \text{poor solvent,} & \beta \ll -1 \end{cases} \quad (A15)$$

thus defining the corresponding equilibrium heights $H = \alpha H_\Theta$ as specified in Table 1.

To characterize $\phi(z)$ in these three regimes it is helpful to express eq A13 as

$$\phi(z) = \phi_\Theta \begin{cases} \sqrt{\beta^2 + \alpha^2 u} - \beta & \beta \geq 0 \\[3mm] -\sqrt{\dfrac{\beta^2}{4} + \alpha^2 u} - \beta & \beta < 0 \end{cases} \quad (A16)$$

where $u = 1 - z^2/H^2$. At $T = \Theta$ we recover $\phi_\Theta u^{1/2}$ while the two $|\beta| \gg 1$ profiles are

$$\phi(z) = \phi_\Theta \begin{cases} \beta\sqrt{1 + \left(\dfrac{3\pi}{4}\right)^{2/3} \beta^{-4/3} u} - \beta & \beta \gg 1 \\[4mm] -\sqrt{\dfrac{\beta^2}{4} + \dfrac{\pi^2}{36\beta^4} u} - \beta & \beta \ll -1 \end{cases} \quad (A17)$$

thus leading to Table 1. The vicinity of the Θ temperature, when $\alpha = 1 + 2\beta/\pi$ with $|\beta| \ll 1$, requires however a lengthier discussion. In this case the profile comprises of two regions. An inner region obtains when $\alpha^2 u \gg \beta^2$ or $\alpha^2 u \gg \beta^2/4$ thus leading to $\phi(z) = \phi_\Theta \alpha u^{1/2}$ corresponding to $T = \Theta$. The exterior part for which $\alpha^2 u \ll \beta^2$ or $\alpha^2 u \ll \beta^2/4$ assumes different forms above and below the Θ temperature. In this case the u term is small and

$$\phi(z) = \phi_\Theta \begin{cases} \dfrac{\alpha^2}{2\beta} u & \beta \gtrsim 0 \\[3mm] \dfrac{3|\beta|}{2}\left(1 + \dfrac{2\alpha^2}{3\beta^2} u\right) & \beta \lesssim 0 \end{cases} \quad (A18)$$

Thus, the exterior region for $\beta \gtrsim 0$ exhibits a good solvent form, while for $\beta \lesssim 0$ it exhibits poor solvent form with a concentration step at the outer edge.

The expressions for $\phi(z)$ and $\Pi(z)$ in Table 1 and Table 2 concern $|\beta| \gg 1$ and $\beta = 0$. The analysis of reference[37] yields an explicit expression, eqs A16, for $\phi(z)$ at any β. This is however formulated in terms of a swelling ratio α specified by a nonlinear equation, eq A14, that can be generally solved only numerically. On the other hand, an explicit parametric solution of eq A14

which provides exact (β, α) pairs in terms of an index $0 \leq \chi \leq \pi/2$, is given by

$$\alpha = \sqrt{\frac{\pi}{\lambda}} \sin \chi \quad (A19)$$

$$\beta = \sqrt{\frac{\pi}{\lambda}} \times \begin{cases} \cos \chi & \beta \geq 0 \\[2mm] 2\cos(\pi - \chi) & \beta < 0 \end{cases} \quad (A20)$$

with $\lambda \equiv 2\chi - \sin(2\chi)$ and $\lambda \equiv 2\chi + 5\sin(2\chi)$ for $\beta \geq 0$ and $\beta < 0$, respectively. This exact solution is helpful in obtaining an interpolation formula

$$\alpha \equiv \frac{H}{H_\Theta}$$

$$\approx \begin{cases} 1 + \left(\dfrac{4}{3\beta} + \dfrac{6}{7\beta^{1/3}}\right)^{-1} & \beta \geq 0 \\[4mm] (1 - \pi\beta)^{-1}\left[1 - \tanh\left(\pi\beta - \dfrac{3}{4}\beta\right)\right] & \beta \leq 0 \end{cases}$$
$$(A21)$$

reproducing the exact solution to within less than 2% for any choice of β and exhibiting the correct asymptotic behaviors. Its use in eqs A16 and eq A25 thus leads to essentially exact expressions for $\phi(z)$ formulated in terms of β alone and valid for any β. Similarly it can be used in A25, discussed below, to obtain $\Pi(z)$. As explained in Appendix F, eq A21 is utilized in the numerical calculation producing the results shown in Figures 2−9.

We finally note that α and $\phi(z)$, as obtained above, are specified in terms of three independent parameters

$$\beta \sim \tau/\phi_\Theta, \quad H_\Theta \sim Np^{1/2}a\phi_\Theta, \quad \phi_\Theta \sim (\sigma p^{1/2})^{1/2} \quad (A22)$$

It is thus also possible to use instead the three independent parameters

$$\tau \sim \beta\phi_\Theta, \quad Np^{1/2}a \sim \phi_\Theta/H_\Theta, \quad \sigma p^{1/2} \sim \phi_\Theta^2 \quad (A23)$$

We utilize this last choice in the plots since it corresponds directly to the experimental control parameters.

The Osmotic Pressure Profile. The $\phi(z)$ profiles allow to obtain the corresponding $\Pi(z)$ by utilizing the appropriate limits of $\Pi a^3/k_B T = \tau\phi^2 + 2w\phi^3$. It is however useful to verify these results by comparison to $\Pi(z) = 2k_B T f_{el}(z)$ as given by eq A10 expressed, upon the substitution $t^2 = y$ and $dt = dy/2y^{1/2}$, as

$$f_{el} = \frac{3\pi^2}{8N^2 pa^5} \int_{z^2}^{H^2} \phi(\sqrt{y})\frac{dy}{2} \quad (A24)$$

where $\phi(t)$ is given by eq A10. This leads to

$$\frac{\Pi(z)}{k_B T}$$

$$= \phi_\Theta \frac{3\pi^2}{8N^2 pa^5} \begin{cases} \dfrac{2}{3}H_\Theta^2\beta^3\left[\left(1 + \dfrac{\alpha^2}{\beta^2}u\right)^{3/2} - 1\right] - \beta H^2 u & \beta \geq 0 \\[4mm] -\dfrac{2}{3}H_\Theta^2\dfrac{\beta^3}{8}\left[\left(1 + \dfrac{4\alpha^2}{\beta^2}u\right)^{3/2} - 1\right] - \beta H^2 u & \beta < 0 \end{cases}$$
$$(A25)$$

In a poor solvent $\beta \ll -1$ and $\alpha = -\pi/6\beta$, leading to $4\alpha^2 u \ll \beta^2$ and

$$\frac{\Pi(z)}{k_B T} = \phi_\Theta \frac{\pi^4}{2^6} \frac{H_\Theta^2}{N^2 p a^5 |\beta|} u \left(1 + \frac{\pi^2}{108\beta^4} u\right) \quad \beta \ll -1 \tag{A26}$$

In a good solvent $\alpha \gg 1$, $\beta \gg 1$ with $\alpha^2 u \ll \beta^2$ and eq A25 reduces to

$$\frac{\Pi(z)}{k_B T} = \frac{3}{8} \pi \frac{H_\Theta}{N\Sigma p a^2} \frac{\alpha^4}{\beta} u^2 \quad \beta \gg 1 \tag{A27}$$

For $\beta = 0$ the term in square brackets is $(2H_\Theta^2/3)u^{3/2}$ thus specifying $\Pi(z)$ at the Θ temperature.

In the vicinity of the Θ temperature we can again distinguish two regions. In the interior region, $\alpha^2 u \gg \beta^2$ for $\beta \geq 0$ and $4\alpha^2 u \gg \beta^2$ for $\beta < 0$, we thus obtain Θ like behavior

$$\frac{\Pi(z)}{k_B T} = \frac{\pi^2}{4Npa^5} \phi_\Theta H_\Theta^2 \alpha^3 u^{3/2} \quad |\beta| \ll 1 \tag{A28}$$

as summarized in Table 2. For the exterior region $\alpha^2 u \ll \beta^2$ or $4\alpha^2 u \ll \beta^2$. Keeping track of second order terms in the expansion, $\Pi(z)$ is given by

$$\frac{\Pi(z)}{k_B T} = \phi_\Theta \frac{3\pi^2}{8Npa^5} \begin{cases} \frac{1}{4} H_\Theta^2 \frac{\alpha^4}{\beta} u^2 & \beta \geq 0, \frac{\alpha^2}{\beta^2} u \ll 1 \\ -\frac{3}{2} H_\Theta^2 \beta \alpha^2 u & \beta < 0, \frac{4\alpha^2}{\beta^2} u \ll 1 \end{cases} \tag{A29}$$

corresponding respectively to good and poor solvent behavior.

■ APPENDIX B: ON $\delta_o(R)$ WITHIN THE SCF THEORY

The leading features of the SCF $\delta_o(R)$, as plotted in Figure 5, can be rationalized by considering the large and small R limits. For brevity we only consider good and poor solvents. To gain a rough understanding of the trends followed by $\delta_o(R)$ we express eq 13, utilizing $dz/du = -H_i/2(1-u)^{1/2}$, as

$$\delta_o(R) = \frac{H_i}{2} \frac{I_{num}^2}{I_{den}} \tag{B1}$$

where

$$I_{num} \equiv \int_0^1 \exp[-r_{ins}^3 u^{n_i+1}] u^{n_i} (1-u)^{-1/2} \, du \tag{B2}$$

and

$$I_{den} \equiv \int_0^1 \exp[-r_{ins}^3 u^{n_i+1}]^2 u^{2n_i} (1-u)^{-1/2} \, du \tag{B3}$$

such that $n_g = 1$ in good solvent, $n_p = 0$ in poor solvent and $r_{ins} \equiv R/R_{ins}$. Note first that both I_{num} and I_{den} depend only on R_{ins} which, in turn, is independent of N. Accordingly, $\delta_o(R) \sim N$ because $\delta_o(R) \sim H_i$. With regard to the dependence of $\delta_o(R)$ on solvent quality we first consider small particle with $r_{ins} \ll 1$ when the $\exp(-r_{ins}^3 u^{n_i+1})$ factor is of order unity thus leading to $\delta_o(R) \sim H_i$. Accordingly $\delta_o(R)$ increases with the solvent quality for $R \ll R_{ins}$. In the opposite limit of $R \gg R_{ins}$ the behavior of $\delta_o(R)$ is modified by additional r_{ins} dependence arising from I_{num}^2/I_{den}.

In this regime the particles are highly localized at the exterior edge and $(1-u)^{-1/2} \approx 1$. Accordingly for good solvent $I_{num} = \int_0^1 \exp[-r_{ins}^3 u^2] u \, du = [1 - \exp(-r_{ins}^3)]/2r_{ins}^3 \sim 1/r_{ins}^3$ and $I_{den} = \int_0^1 \exp[-r_{ins}^3 u^2] u^2 \, du = [(2\pi)^{1/2} \text{erf}(2^{1/2} r_{ins}^{3/2}) - 4r_{ins}^{3/2} \exp(-2r_{ins}^3)]/16r_{ins}^{9/2} \sim 1/r_{ins}^{9/2}$ while for poor solvents $I_{num} = \int_0^1 \exp[-r_{ins}^3 u] \, du = [1 - \exp(-r_{ins}^{3/2})]/r_{ins}^3 \sim 1/r_{ins}^3$ and $I_{den} = \int_0^1 \exp[-r_{ins}^3 u^2]^2 \, du = [1 - \exp(-2r_{ins}^3)]/2r_{ins}^3 \sim 1/r_{ins}^3$. Thus, $\delta_o(R)$ in the $R \gg R_{ins}$ case follows

$$\delta_o(R) \sim \begin{cases} \frac{H_g R_{ins}^{3/2}(g)}{R^{3/2}} \sim \frac{N\tau^{1/6}}{R^{3/2}\sigma^{1/3}} & \beta \gg 1 \\ \frac{H_p R_{ins}^3(p)}{R^3} \sim \frac{N|\tau|^0}{R^3\sigma} & \beta \ll -1 \end{cases} \tag{B4}$$

since for good solvent $H_g \sim \tau^{1/3}\sigma^{1/3}$ and $R_{ins}(g) \sim \tau^{-1/9}\sigma^{-4/9}$ while for poor solvent $H_p \sim |\tau|^{-1}\sigma$ and $R_{ins}(p) \sim |\tau|^{1/3}\sigma^{-2/3}$. $\delta_o(R)$ increases with solvent quality also in $R \gg R_{ins}$ limit.

■ APPENDIX C: THE MAXIMUM IN $c_{prt}(z)$ FOR TERNARY ADSORPTION

The maximum in $c_{prt}(z)$ for ternary adsorption, as specified by $\partial c_{prt}(z)/\partial z = 0$, occurs at

$$z_{MAX}(i)$$
$$= \begin{cases} H_g \sqrt{1 - \frac{1}{2} \frac{R_{co}(g)}{R}} & \beta \gg 1, \frac{R_{co}(g)}{R} < 2 \\ H_\Theta \sqrt{1 - \frac{1}{3} \frac{R_{co}(\Theta)}{R}} & \beta = 0, \frac{R_{co}(\Theta)}{R} < 3 \\ H_p & \beta \ll -1 \end{cases} \tag{C1}$$

and the corresponding maximal value of $c_{prt}(z)$ is given by

$$\frac{c_{prt}(z_{MAX}(i))}{c_b} = \begin{cases} \exp\left[\frac{1}{4} \frac{RR_{co}(g)}{R_{att}^2(g)}\right] & \beta \gg 1 \\ \exp\left[\frac{2}{3^{3/2}} \frac{R^{3/2} R_{co}^{1/2}(g)}{R_{att}^2(g)}\right] & \beta = 0 \\ \exp\left[\frac{R^2}{R_{att}^2(g)}\right] & \beta \ll -1 \end{cases} \tag{C2}$$

■ APPENDIX D: TERNARY ADSORPTION BEHAVIOR IN THE $R \gg R_{co}(i)$ LIMIT

The altitude $z_{co}(i)$ in the limit of $R \gg R_{co}(i)$, easily realized in the good solvent regime, is given by $z_{co}(i)/H_i \approx 1 - R_{co}(i)/2R$ and the particles adsorb within a a narrow exterior region of thickness $\delta_{tern}(i) = H_i - z_{co}(i)$

$$\delta_{tern}(i) \approx \frac{H_i}{2} \frac{R_{co}(i)}{R} \sim Na \begin{cases} \varepsilon/R\sigma^{1/3} & \beta \gg 1 \\ \varepsilon/R\sigma^{1/2} & \beta = 0 \\ \varepsilon/R\sigma & \beta \ll -1 \end{cases} \tag{D1}$$

with $\delta_{tern}(p) > \delta_{tern}(\Theta) > \delta_{tern}(g)$. In contrast to $\delta_{ins}(i)$ all $\delta_{tern}(i) \sim \varepsilon/R$ and they differ only in their σ dependence. The corresponding expressions for $c_{prt}(z)$, when the exponent in eq 21

is dominated by the second term, are

$$
\frac{c_{prt}(z)}{c_b}
$$

$$
= \begin{cases}
\exp\left\{-\left[\dfrac{R}{R_{att}(g)}\right]^2 \dfrac{R_{co}(g)}{R}\left(\dfrac{H_g - z}{\delta_{tern}(g)}\right)^2\right\} & \beta \gg 1 \\[2em]
\exp\left\{-\left[\dfrac{R}{R_{att}(\Theta)}\right]^2 \left(\dfrac{R_{co}(\Theta)}{R}\right)^{1/2}\left(\dfrac{H_\Theta - z}{\delta_{tern}(\Theta)}\right)^{3/2}\right\} & \beta = 0 \\[2em]
\exp\left\{-\left[\dfrac{R}{R_{att}(p)}\right]^2 \dfrac{H_p - z}{\delta_{tern}(p)}\right\} & \beta \ll -1
\end{cases}
$$

$$\text{(D2)}$$

The powers of $(H_i - z)$ in the exponent are identical to those found in eq 11 and the expression differ in that $\delta_{tern}(i)$ replaces $\delta_{ins}(i)$ and by the appearance of a prefactor. Similarly, the position of the maximal $c_{prt}(z)$ for good and Θ solvents in this limit can be specified as a depth $\Delta(i) = H_i - z_{MAX}(i) \sim \delta_{tern}(i)$

$$
\Delta(i) = \begin{cases}
\dfrac{H_g}{4}\dfrac{R_{co}(g)}{R} = \dfrac{1}{2}\delta_{tern}(g) & \beta \gg 1 \\[1.5em]
\dfrac{H_\Theta}{6}\dfrac{R_{co}(\Theta)}{R} = \dfrac{1}{3}\delta_{tern}(\Theta) & \beta = 0
\end{cases}
\tag{D3}
$$

■ APPENDIX E: ON THE TERNARY ADSORPTION Γ

In the following we consider the small and large R limits of Γ for good and poor solvents. For brevity we will not discuss the Θ solvent case. To this end, it is useful to express eq 21 in the form

$$
\frac{c_{prt}(z)}{c_b} = \exp\{r_{att}^2(i)[u^{n_i} - r_{co}(i)u^{n_i + 1}]\} \tag{E1}
$$

where $n_g = 1$, $n_\Theta = 1/2$ and $n_p = 0$ introducing for compactness the notation $r_{att}(i) = R/R_{att}(i)$ and $r_{co}(i) = R/R_{co}(i)$ such that $r_{ins}^3(i) = r_{att}^2(i)r_{co}(i)$. In turn, Γ as defined by eq 22 may be written, utilizing $dz = -(H_i/2)(1 - u)^{-1/2}$, in the form

$$
\frac{\Gamma_i}{c_b H_i} = \int_0^1 \frac{\exp[r_{att}^2(i)(u^{n_i} - r_{co}(i)u^{n_i + 1})]}{2\sqrt{1 - u}}\, du \tag{E2}
$$

so that Γ_i/H_i is a function of $r_{att}(i)$ and $r_{co}(i)$ alone.

Small R: $r_{att} \ll 1$ and $r_{ins} \ll 1$ Expanding $\exp[r_{att}^2(i)(u^{n_i} - r_{co}(i)u^{n_i+1})]$ leads to integrals of the form $\int_0^1 u^q(1 - u)^{-1/2}\, du = \pi^{1/2}q!/(q + 1/2)!$. Evaluation of Γ_i for $r_{ins}(i) \ll r_{att}(i) \ll 1$ or $R_{ins}(i) \gg R_{att}(i) \gg R$ leads to

$$
\frac{\Gamma_i}{c_b H_i} \approx \begin{cases}
1 + \dfrac{2}{3}r_{att}^2(g) & \beta \gg 1 \\[1em]
1 + r_{att}^2(p) & \beta \ll -1
\end{cases}
\tag{E3}
$$

In the $r_{att}(i) \ll r_{ins}(i) \ll 1$ or $R_{att}(i) \gg R_{ins}(i) \gg R$ limit, the attractive interactions are negligible compared to the insertion penalty and

$$
\frac{\Gamma_i}{c_b H_i} \approx \begin{cases}
1 - \dfrac{8}{15} r_{ins}^3(g) & \beta \gg 1 \\[1em]
1 - \dfrac{2}{3} r_{ins}^3(p) & \beta \ll -1
\end{cases}
\tag{E4}
$$

In both cases, Γ is dominated by H_i and accordingly $\Gamma_p \sim H_p < \Gamma_g \sim H_g$. The relative amplitude of R_{ins} and R_{att} is manifested in

$\Gamma_i/c_b H_i$ comparing Γ_i to the particle concentration in a brush free region of identical volume. When $R_{ins} \gg R_{att} \gg R$ attractive interactions play a role and $\Gamma_i > c_b H_i$. In contrast the insertion penalty dominates when $R_{att} \gg R_{ins} \gg R$ thus leading to depletion $\Gamma_i < c_b H_i$.

Large R: $r_{att} > 1$. The case $R > R_{att}$ typically involves two scenarios as illustrated in Figure 9: (a) In a poor solvent, $R_{co}(p) \gg R > R_{ins}(p) \gg R_{att}(p)$ or $r_{co}(p) \ll 1$ with $r_{att}(p) \gg r_{ins}(p) > 1$: (b) In a good solvent, $R > R_{att}(g) \gg R_{ins}(g) \gg R_{co}(g)$ or $r_{co}(g) \gg r_{ins}(g) \gg r_{att}(g) > 1$.

In the first situation $r_{co}(p) \ll 1$ and eq E2 may be approximated by

$$
\frac{\Gamma_p}{c_b H_p} = \exp[r_{att}^2(p)]\int_0^1 \frac{du}{2\sqrt{1 - u}}
$$

$$
= \frac{\exp[r_{att}^2(p)]}{3} \quad \beta \ll -1 \tag{E5}
$$

thus leading to $\Gamma_p \sim H_p \exp(|\tau|\varepsilon R^2)$ increasing with decreasing solvent quality.

In the second, good solvent case the particles are localized at the brush periphery and $(1 - u)^{1/2} \approx 1$ thus allowing to approximate eq E2 by

$$
\frac{\Gamma_g}{c_b H_g} = \int_0^1 \exp[r_{att}^2(g)u]\exp(-r_{ins}^3(g)u^2)\, du \quad \beta \gg 1
$$

$$
= \frac{\sqrt{\pi}}{4r_{ins}^{3/2}(g)}\exp\left[\frac{r_{att}^2(g)}{4r_{co}(g)}\right]\left[\mathrm{erf}\left(\frac{r_{att}(g)}{2r_{co}^{1/2}(g)}\right)\right.
$$

$$
\left. + \mathrm{erf}\left(\frac{r_{att}(g)[2r_{co}(g) - 1]}{2r_{co}^{1/2}(g)}\right)\right] \tag{E6}
$$

where the second erf term can be approximated by $\mathrm{erf}(r_{att}(g)r_{co}^{1/2}(g)) \approx 1$ and since $\mathrm{erf}(x) \in [0,1]$

$$
\frac{\Gamma_g}{c_b} \approx \frac{H_g}{r_{ins}^{3/2}(g)}\exp\left[\frac{r_{att}^2(g)}{4r_{co}(g)}\right]
$$

$$
= H_g\left(\frac{R_{ins}(g)}{R}\right)^{3/2}\exp\left[\frac{RR_{co}(g)}{4R_{att}^2(g)}\right] \quad \beta \gg 1 \tag{E7}
$$

where $RR_{co}(g)/R_{att}^2(g) \sim R\varepsilon^2/\tau$ thus leading to $\Gamma_g \sim \exp(R\varepsilon^2/\tau) \ll \Gamma_p \sim \exp(|\tau|\varepsilon R^2)$ for sufficiently large R. The limits discussed in this appendix are illustrated in Fig. 9.

■ APPENDIX F: DEFINITIONS AND DETAILS OF THE NUMERICAL IMPLEMENTATION

The discussion in the body of the text aimed at identification of trends and the characteristic R's. It was thus focused on the $\beta = 0$ and $|\beta| \gg 1$ regimes using approximations assuming slow variation of $\phi(z)$ and $\Pi(z)$. In practical terms these approximations, while leading to simple expressions, incur a price: (i) Attaining $|\beta| \gg 1$ for typical τ, w requires low σ values within the brush regime i.e., with strongly crowded chains. Accordingly $|\beta| \gg 1$ may require high N values that are difficult to access in experiment or simulation. (ii) The approximations ignore numerical factors, of importance in considering the regime boundaries, as well as the effects due to partial insertion at the brush periphery. Also, the validity of the assumption of slowly varying $\Pi(z)$ changes with the solvent quality. To circumvent these

difficulties we base the calculations producing the figures on the unapproximated eq 1 and consider a broader range of β values such that the shown results represent exact solutions for the SCF equations. The simple algorithm utilized is described below. It takes into account numerical factors omitted in the main body of the article.

1. Calculation of $\phi(z)$ and $\Pi(z)$. The $\phi(z)$ profiles are obtained from eq A13 upon substitution of H_Θ (defined in Table 1), and of the interpolation formula A21 for $\alpha(\beta)$ specified by the single "solvent quality" parameter β defined in eq 3; the brush height is obtained via $H = \alpha H_\Theta$. The use of the exact parametric solution A20 instead of the interpolation formula yields indistinguishable results. With the so-obtained analytical $\phi(z)$ at hand, we evaluate the osmotic pressure profile via $a^3\Pi(z)/k_BT = \tau\phi^2(z) + 2w\phi^3(z)$. The $\phi(z)$ and $a^3\Pi(z)/k_BT$ profiles characterizing the particle-free brush are fully determined by τ, w, and the effectively only two additional parameters of the SCF theory: the reduced length $z/Np^{1/2}a$, and the reduced surface density $\sigma/p^{1/2}$. Plots of $\phi(z)$ and $a^3\Pi(z)/k_BT$ vs $z/Np^{1/2}a$ and for a given $\sigma/p^{1/2}$ are thus independent of a, p, and N.

2. Definitions and Calculation of $F_{ins}(z)$, $F_{att}(z)$, $F_{tern}(z)$, and $c_{prt}(z)$ Profiles. The particle concentration profile $c_{prt}(z)/c_b \equiv \exp(-F(z)/k_BT)$ where $F(z) \equiv F_{ins}(z) + F_{att}(z)$ is a free energy of a particle with its geometrical center at altitude z. F_{att} can take different forms depending on the mode, as specified below, while F_{ins} is uniquely defined by eq 1. For a spherical particle of radius R the profile $c_{prt}(z)$ identically vanishes for $z < R$, the remainder of this paragraph solely addresses the case $z \geq R$. The cross sectional volume required to evaluate eq 1 is $A(z,z')\,dz' = \pi(R + z - z')(R - z + z')dz'$ if $|z' - z| \leq R$ and $A(z,z') = 0$ otherwise. Note that when $\Pi(z) \approx \Pi(z \pm R)$ the insertion free energy reduces to $F_{ins}(z) \approx \Pi(z)V$ because $\int_0^\infty A(z,z')\,dz' = (4/3)\pi R^3 = V$ is the volume of a sphere. The different F_{att} considered are as follows: (i) non-adsorbing particles, $F_{att}(z) \equiv 0$; (ii) primary adsorption, $F_{att}(z) \equiv -Ek_BT$ for $R < z < R + \Delta R$ and vanishing otherwise, for the figures we use $\Delta R = a$; (iii) weak monomer-particle attraction: $F_{att}(z) \equiv -\varepsilon a^{-2}\int_0^\infty L(z,z')\phi(z')\,dz'$ where $L(z')\,dz'$ is the surface area of an infinitesimal stripe at height z'. For a sphere $L(z') = 2\pi R$ if $|z' - z| \leq R$ and $L_z(z') = 0$ otherwise. Note that when $\phi(z) \approx \phi(z \pm R)$ this attractive term is approximated by $F_{att}(z) \approx -\varepsilon 4\pi\phi(z)(R/a)^2$ because $\int_0^\infty L(z, z')\,dz = 4\pi R^2$ is the surface area of a sphere. (iv) In the general case, not discussed in the manuscript, F_{att} comprises a sum of the three aforementioned terms and may exhibit additional contributions such as van der Waals attraction between the particle and the surface. These explicit expressions and the exact $\phi(z)$ and $\Pi(z)$ allow to calculate $F(z)$, $c_{prt}(z)$, δ_o defined in eq 13 and $\Gamma \equiv \int_0^{H+R}c_{prt}(z)\,dz$ for given brush parameters, supplemented by R and ε or E values, by a simple numerical integration. To this end we discretize $z \in [0,H+R]$ into 10 000 bins, and evaluate all integrals by summing over bins.

3. Definition of the Characteristic Radii R_{ins}, R_{att}, R_{co}, and R_{prim}. The characteristic R are defined by for a hypothetical state of a particle experiencing insertion at $z = 0$ conditions. Hard-core spherical particles cannot approach the grafting surface to $0 < z < R$ and $c_{prt}(z) \equiv 0$ in this range. The hard core interaction is not explicitly accounted in the $F(z)$ as defined above. To define the characteristic radii we introduce the following notation: $F_{ins}(0) \equiv \Pi(0)V$, $F_{prim} \equiv F_{ins}(0) - Ek_BT$, $F_{att}(0) \equiv -\varepsilon a^{-2}\phi(0)4\pi R^2$, and $F_{tern}(0) \equiv F_{ins}(0) + F_{att}(0)$. In the insertion limit, when $R \ll H$ such that $\phi(z)$ and $\Pi(z)$ are slowly varying over a distance R, the

hereby defined energies are close to the corresponding free energy values at grazing contact, $z = R$.

Characteristic length scales were discussed in the text for $\beta = 0$ $(i = \Theta)$, $\beta \gg 1$ $(i = g)$, and $\beta \ll -1$ $(i = p)$ while omitting numerical prefactors. In the numerical calculations we also consider intermediate β values and incorporate numerical factors, that affect the boundaries between the regimes. Generalized characteristic length scales are thus required and defined using the above $F(0)$'s as follows: (i) R_{ins} is obtained from $F_{ins}(0)/k_BT = 1$, or equivalently $R_{ins}/a \equiv (4\pi\Pi(0)/3k_BT)^{1/3}$, (ii) R_{att} is specified via $F_{att}(0)/k_BT = -1$, that is $R_{att}/a \equiv [4\pi\varepsilon\phi(0)]^{-1/2}$, (iii) R_{co} is introduced via $F_{tern}(0)/k_BT = 0$, yielding $R_{co} \equiv R_{ins}^3/R_{att}^2$, cf. eq 19, and (iv) R_{prim} is defined by $F_{prim}/k_BT = 0$, i.e. $R_{prim} \equiv E^{1/3}R_{ins}$.

■ AUTHOR INFORMATION

Corresponding Author
*E-mail: (A.H.) avraham.halperin@ujf-grenoble.fr; (E.B.Z.) kzhulina@hotmail.com; (M.K.) mk@mat.ethz.ch.

■ REFERENCES

(1) Gupta, P. S.; Agrawal, M.; Uhlmann, P.; Simon, F.; Oertel, U.; Stamm, M. *Macromolecules* **2008**, *41*, 8152–8158.

(2) Uhlmann, P.; Merlitz, H.; Sommer, J.-U.; Stamm, M. *Macromol. Rapid Commun.* **2009**, *30*, 732–740.

(3) Tokareva, I.; Minko, S.; Fendler, J. H.; Hutter, E. *J. Am. Chem. Soc.* **2004**, *126*, 15950–15951.

(4) Liu, Z.; Pappacena, K.; Cerise, J.; Kim, J.; Durning, C. J.; O'Shaughnessy, B.; Levicky, R. *Nano Lett.* **2002**, *2*, 219.

(5) Bhat, R. R.; Tomlinson, M. R.; Genzer, J. *Macromol. Rapid Commun.* **2004**, *25*, 270–274.

(6) Kim, J. U.; O'Shaughnessy, B. *Macromolecules* **2006**, *39*, 413–425.

(7) Hamdoun, B.; Ausserre, D.; Cabuil, V.; Joly, S. *J. Phys. II Fr.* **1996**, *6*, 503–510.

(8) Lauter-Pasyuk, V.; Lauter, H. J.; Ausserre, D.; Gallot, Y.; Cabuil, V.; Kornilov, E. I.; Hamdoun, B. *Physica B* **1998**, *241−243*, 1092–1094.

(9) Thompson, R. B.; Ginzburg, V. V.; Matsen, M. W.; Balazs, A. C. *Science* **2001**, *292*, 2469.

(10) Huh, J.; Ginzburg, V. V.; Balazs, A. C. *Macromolecules* **2000**, *33*, 8085–8096.

(11) Arita, T.; Yoshimura, T.; Adschiri, T. *Nanoscale* **2010**, *2*, 1467–1473.

(12) Elbert, D. L.; Hubbell, J. A. *Annu. Rev. Mater. Sci.* **1996**, *26*, 365–394.

(13) Lee, H. J.; Lee, H. B.; Andrade, J. D. *Prog. Polym. Sci.* **1995**, *20*, 1043–1079.

(14) (a) Harris, J. M., Ed. *Poly(Ethylene Glycol) Chemistry: Biotechnical and Biomedical Applications*; Plenum Press: New York, 1992; (b) Harris, J. M., Zalipsky, S., Eds. *Poly(Ethylene Glycol) Chemistry and*

Biological Applications; American Chemical Society: Washington DC, 1997.

(15) Cole, M. A.; Voelcker, N. H.; Thissen, H.; Griesser, H. J. *Biomaterials* **2009**, *30*, 1827.

(16) Kikuchi, A.; Okano, T. *Prog. Polym. Sci.* **2002**, *27*, 1165.

(17) Cooperstein, M. A.; Canavan, H. E. *Langmuir* **2010**, *26*, 7695.

(18) Jeon, S. I.; Lee, J. H.; Andrade, J. D.; de Gennes, P.-G. *J. Colloid Interface Sci.* **1991**, *142*, 149–158.

(19) Szleifer, I. *Biophys. J.* **1997**, *72*, 595–612.

(20) Currie, E. P. K.; Van der Gucht, J.; Borisov, O. V.; Cohen Stuart, M. A. *Pure Appl. Chem.* **1999**, *71*, 1227–1241.

(21) Currie, E. P. K.; Norde, W.; Cohen Stuart, M. A. *Adv. Colloid Sci.* **2003**, *100−102*, 205–265.

(22) Halperin, A. *Langmuir* **1999**, *15*, 2525–2533.

(23) Halperin, A.; Fragneto, G.; Schollier, A.; Sferrazza, M. *Langmuir* **2007**, *23*, 10603–10617.

(24) Halperin, A.; Kröger, M. *Langmuir* **2009**, *25*, 11621–11634.

(25) Ermilov, V.; Lazutin, A.; Halperin, A. *Macromolecules* **2010**, *43*, 3511–3520.

(26) Steels, B. M.; Koska, J.; Haynes, C. A. *J. Chromatogr. B* **2000**, *743*, 41–56.

(27) Milchev, A.; Dimitrov, D. I.; Binder, K. *Polymer* **2008**, *49*, 3611.

(28) Yaneva, J.; Dimitrov, D. I.; Milchev, A.; Binder, K. *J. Colloid Interface Sci.* **2009**, *336*, 51–58.

(29) Halperin, A.; Zhulina, E. B. *Langmuir* **2010**, *26*, 8933–8940.

(30) Murat, M.; Grest, G. S. *Macromolecules* **1996**, *29*, 8282–8284.

(31) Fredrickson, G. H.; Ajdari, A.; Leibler, L.; Carton, J.-P. *Macromolecules* **1992**, *25*, 2882–2889.

(32) Williams, D. R. M. *Macromolecules* **1993**, *26*, 5096–5098.

(33) Subramanian, G.; Williams, D. R. M.; Pincus, P. A. *Macromolecules* **1996**, *29*, 4045–4050.

(34) Yang, J.; Yamato, M.; Okano, T. *MRS Bull.* **2005**, *30*, 189.

(35) da Silva, R. M. P.; Mano, J. F.; Reis, R. L. *Trends Biotechnol.* **2007**, *25*, 577.

(36) Chiu, J. J.; Kim, B. J.; Yi, G.-R.; Bang, J.; Kramer, E. J.; Pine, D. J. *Macromolecules* **2007**, *40*, 3361–3365.

(37) Zhulina, E. B.; Borisov, O. V.; Priamitsyn, V. A. *J. Colloid Interface Sci.* **1990**, *137*, 495–511.

(38) Milner, S. T.; Witten, T. A.; Cates, M. E. *Macromolecules* **1988**, *21*, 2610–1619.

(39) Milner, S. T. *Science* **1991**, *251*, 905–914.

(40) Toomey, R.; Tirrell, M. *Annu. Rev. Phys. Chem.* **2008**, *59*, 493.

(41) Karim, A.; Satija, S. K.; Douglas, J. F.; Ankner, J. F.; Fetters, L. J. *Phys. Rev. Lett.* **1994**, *73*, 3407.

(42) Wagner, M.; Brochard Wyart, F.; Hervet, H.; de Gennes, P.-G. *Colloid Polym. Sci.* **1993**, *271*, 621.

(43) Baulin, V. A.; Halperin, A. *Macromol. Theory Simul.* **2003**, *12*, 549–559.

(44) Baulin, V. A.; Zhulina, E. B.; Halperin, A. *J. Chem. Phys.* **2003**, *119*, 10977–10988.

(45) (a) Yim, H.; Kent, M. S.; Satija, S.; Mendez, S.; Balamurugan, S. S.; Balamurugan, S.; Lopez, G. P. *Phys. Rev. E* **2005**, *72*, 051801. (b) Yim, H.; Kent, M. S.; Mendez, S.; Lopez, G. P.; Satija, S.; Seo, Y. *Macromolecules* **2006**, *39*, 3420–3426.

(46) Koga, T.; Tanaka, F.; Motokawa, R.; Koizumi, S.; Winnik, F. M. *Macromolecules* **2008**, *41*, 9413.

(47) In our treatment, $\varepsilon \ll 1$ has no effect on $\phi(z)$. The effect of $\varepsilon \ll 1$ on $\phi(z)$ is negligible when $\phi(z)$ is higher than ϕ_{ads} associated with the adsorbed layer. Within the SCF theory the chains are Gaussian. Accordingly, ϕ_{ads} can be roughly estimated by considering the adsorption of a Gaussian chain onto a planar surface when each monomer at the surface gains $\varepsilon k_B T$. An adsorbed chain forming a layer of thickness D is assumed to have Na/D attractive surface contacts thus leading to $D \approx a/\varepsilon$.[60] Consequently $\phi_{ads} \approx \varepsilon$ since the area per adsorbed Gaussian chain remains Na^2. Accordingly, $\varepsilon \ll 1$ may affect the distal part of the SCF $\phi(z)$ in good and Θ solvent but will have negligible effects on the distal part of $\phi(z)$ in a poor solvent providing $\phi_p \approx \bar{\phi}_p > \phi_{ads}$.

(48) The terms primary and ternary adsorption for adsorption at the wall and within the brush were introduced in the context of protein-brush interactions.[21]

(49) Grosberg, A. Yu.; Khokhlov, A. R. *Statistical Physics of Macromolecules*; American Institute of Physics: New York, 1994.

(50) The chemical potential of component i is specified in terms of dimensionless activity $a_i = \gamma_i c_i / c_i^o$ where c_i is the molar concentration, $c_i^o = 1$ mol/liter corresponding to a hypothetical standard state exhibiting Henry's law and γ_i is an activity coefficient such that $\gamma_i \rightarrow 1$ when $c_i \rightarrow 0$.[59] Accordingly, the numerical value of a_i for a dilute solution is identical to the dimensionless value of the molar c_i. To simplify the notation we thus denote the activity by the corresponding c_i.

(51) Guskova, A.; Pal, S.; Seidel, C. *Europhys. Lett.* **2009**, *88*, 38006.

(52) In an athermal solvent, $F_{ins} \approx \Pi R^3$ is applicable for R larger than the blob size ζ as discussed in (a) de Gennes, P.-G. *C. R. Acad. Sci. Paris, Ser. B* **1979**, *288*, 359. (b) Odijk, T. *Macromolecules* **1996**, *29*, 1842.

(53) In the $\beta \ll -1$, case $\phi(z) = \phi_p(1 - u/54\beta^4)$ and $F_{tern} = F_{att} + F_{ins}$ is $F_{tern}(z)/k_B T = -\varepsilon\phi_p R^2/a^2 + (3/8)\pi^2(R^3/a^3)(\sigma^2/p\phi_p)(1 - \varepsilon a/2R\phi_p^3)u$. However, the u-dependent term is dominated by the osmotic contribution because $\varepsilon a/2R\phi_p^3 \ll 1$ thus leading to eq 17.

(54) Filippidi, E.; Michailidou, V.; Loppinet, B.; Rühe, J.; Fytas, G. *Langmuir* **2007**, *23*, 5139–5142.

(55) Bockstaller, M. R.; Thomas, E. L. *Phys. Rev. Lett.* **2004**, *93*, 166106.

(56) Chium, J. J.; Kim, B. J.; Yi, G.-R.; Bang, J.; Kramer, E. J.; Pine, D. J. *Macromolecules* **2007**, *40*, 3361–3365.

(57) Liu, Z.; Pappacena, K.; Cerise, J.; Kim, J.; Durning, C. J.; O'Shaughnessy, B.; Levicky, R. *Nano Lett.* **2002**, *2*, 219.

(58) Balazs, A. C.; Emrick, T.; Russell, T. P. *Science* **2006**, *314*, 1107.

(59) *Quantities, Units and Symbols in Physical Chemistry—The IUPAC Green Book*, 3rd ed.; Royal Society of Chemistry: London, 2007.

(60) de Gennes, P.-G. *Scaling Concepts in Polymer Physics*; Cornell University Press: Ithaca, NY, 1979.